Nucleus of the Solitary Tract in the C57BL/6J Mouse: Subnuclear Parcellation, Chorda Tympani Nerve Projections, and Brainstem Connections

Donald Ganchrow,[1] Judith R. Ganchrow,[2] Vanessa Cicchini,[3] Dianna L. Bartel,[4] Daniel Kaufman,[3] David Girard,[3] and Mark C. Whitehead[3]*

[1]Department of Anatomy and Anthropology, Sackler Faculty of Medicine, Tel-Aviv University, 69978 Ramat Aviv, Tel-Aviv, Israel
[2]Institute of Dental Sciences, The Hebrew University-Hadassah School of Dental Medicine Founded by the Alpha Omega Fraternity, 91120 Jerusalem, Israel
[3]Division of Anatomy, MC 0604, Department of Surgery, School of Medicine, University of California, San Diego, La Jolla, California 92037
[4]Rocky Mountain Taste and Smell Center, Department of Cell and Development Biology, University of Colorado Anschutz Medical Center, Aurora, Colorado 80045

ABSTRACT

The nucleus of the solitary tract (NST) processes gustatory and related somatosensory information rostrally and general viscerosensory information caudally. To compare its connections with those of other rodents, this study in the C57BL/6J mouse provides a subnuclear cytoarchitectonic parcellation (Nissl stain) of the NST into rostral, intermediate, and caudal divisions. Subnuclei are further characterized by NADPH staining and $P2X_2$ immunoreactivity (IR). Cholera toxin subunit B (CTb) labeling revealed those NST subnuclei receiving chorda tympani nerve (CT) afferents, those connecting with the parabrachial nucleus (PBN) and reticular formation (RF), and those interconnecting NST subnuclei. CT terminals are densest in the rostral central (RC) and medial (M) subnuclei; less dense in the rostral lateral (RL) subnucleus; and sparse in the ventral (V), ventral lateral (VL), and central lateral (CL) subnuclei. CTb injection into the PBN retrogradely labels cells in the aforementioned subnuclei; RC and M providing the largest source of PBN projection neurons. Pontine efferent axons terminate mainly in V and rostral medial (RM) subnuclei. CTb injection into the medullary RF labels cells and axonal endings predominantly in V at rostral and intermediate NST levels. Small CTb injections within the NST label extensive projections from the rostral division to caudal subnuclei. Projections from the caudal division primarily interconnect subnuclei confined to the caudal division of the NST; they also connect with the area postrema. $P2X_2$-IR identifies probable vagal nerve terminals in the central (Ce) subnucleus in the intermediate/caudal NST. Ce also shows intense NADPH staining and does not project to the PBN. J. Comp. Neurol. 522:1565–1596, 2014.

INDEXING TERMS: cholera toxin B; fungiform taste bud; solitary nucleus atlas and projections; taste; Nissl; cytoarchitectonics

The brainstem nucleus of the solitary tract (NST) is a second-order subnuclear complex that processes both gustatory and related somatosensory and general viscerosensory, peripheral afferent information in its respective rostral and caudal regions. By forming connections that differentially engage pathways ascending to the pontine parabrachial nucleus (PBN) and project locally to the reticular formation (RF) or intranuclearly within NST, the NST subnuclei mediate taste perception, salivation, lingual/facial movements, swallowing, and esophagogastrointestinal reflexes. Previously

Grant sponsor: National Institutes of Health; Grant number: F31 DC009762 (to D.L.B.); Grant number: R01 33506 (to M.C.W.); Grant number: R56 DC000147 (to Thomas E. Finger); Grant number: P30 DC004657 (to Thomas E. Finger).

*CORRESPONDENCE TO: Mark C. Whitehead, Division of Anatomy, MC 0604, Department of Surgery School of Medicine, University of California, San Diego, La Jolla, CA. E-mail: mcwhitehead@ucsd.edu

Received April 16, 2013; Accepted October 8, 2013.
DOI 10.1002/cne.23484
Published online October 22, 2013 in Wiley Online Library (wileyonlinelibrary.com)

reported in other rodents, afferents and efferents of the NST subnuclei are only beginning to be addressed in a murine model (for review see Whitehead and Finger, 2008; rat: Contreras et al., 1982; Ross et al., 1985; Altschuler et al., 1989; Cunningham and Sawchenko, 1989; Herbert et al., 1990; Travers and Norgren, 1995; Hayakawa et al., 2003; May and Hill, 2006; hamster: Whitehead and Frank, 1983; Whitehead, 1990; mouse: Zaidi et al., 2008; Wang and Bradley, 2010).

The mechanisms of gustatory coding have been well described for the peripheral taste system, where the molecular receptors for bitter, sweet, and umami sensing have been identified in specific cell types within the taste buds of transgenic mice (Nelson et al., 2001; for review see Chandrashekar et al., 2006). However, the topographic localization of quality-specific or multiquality taste areas in the NST remains elusive. In part, this is due to the unclear documentation of cytoarchitectonic and subnuclear delineation of labeled NST cells (Sugita and Shiba, 2005; see also Damak et al., 2008; Yamamoto et al., 2011; cf. Ohmoto et al., 2008; Chen et al., 2011). Similarly, in caudal NST of mouse, although general viscerosensory primary afferent terminations and associated circuits are located primarily caudal to rostral gustatory NST (Paton, 1998a,b; Ma et al., 2002; Zhang et al., 2006), cytoarchitectonic subnuclear parcellation related to visceral functions has not been described in detail. A standard reference for the entire NST would facilitate comparisons in both gustatory and related viscerosensory pathways 1) among normal and transgenic strains of mice and 2) between connectional patterns of and molecular marker expression in subnuclei of the NST.

To further these aims, the present study in the C57BL/6J mouse provides a cytoarchitectonic (Nissl stain) parcellation of the entire NST, including its caudal, general viscerosensory region, into subnuclei as presented in a standard coronal series of sections relative to the obex. Previously published reports, including brain atlases specifically in rodents helped inform the present scheme for the mouse NST. Nissl material is supplemented by two chemoarchitectonic markers to characterize further the presently defined NST subnuclei in intermediate and caudal divisions of NST, $P2X_2$ (neurotransmitter receptor for ATP) immunopositivity to demonstrate probable vagal nerve (esophageal) afferent input via the solitary tract into NST at the obex/area postrema (AP) level (Ohmoto et al., 2008) and nicotinamide adenine dinucleotide phosphate (NADPH)-diaphorase to identify NST subnuclei comparable to those in the rat (Herbert et al., 1990). Moreover, by

Abbreviations

Amb	ambiguus nucleus
AP	area postrema
C	central canal
CI	caudal interstitial nucleus of the medial longitudinal fasciculus
CT	chorda tympani nerve
Cu	cuneate nucleus
DC	dorsal cochlear nucleus
DMSp5	dorsomedial spinal trigeminal nucleus
DPGi	dorsal paragigantocellular nucleus
DT	dorsal tegmental nucleus
ECu	external cuneate nucleus
Gi	gigantocellular reticular nucleus
GiA	gigantocellular reticular nucleus, alpha
GiV	gigantocellular reticular nucleus, ventral part
Gr	gracile nucleus
GrC	granular layer of cochlear nuclei
In	intercalated nucleus of medulla
IRt	intermediate reticular nucleus
K	Kölliker-Fuse nucleus (of pons)
LC	locus coeruleus
Li	linear nucleus
LPGi	lateral paragigantocellular nucleus
LRt	lateral reticular nucleus
LRtPC	lateral reticular nucleus, parvicellular part
LVe	lateral vestibular nucleus
m5	motor root of the trigeminal nerve
mlf	medial longitudinal fasciculus
MdD	medullary reticular nucleus, dorsal part
MdV	medullary reticular nucleus, ventral part
MVe	medial vestibular nucleus
MVeMC	medial vestibular nucleus, magnocellular part
MVePC	medial vestibular nucleus, parvocellular part
NST	nucleus of the solitary tract
P7	perifacial zone
Pa5	paratrigeminal nucleus
PBN	parabrachial nucleus (of pons)
PBN-L	parabrachial nucleus, lateral division
PBN-M	parabrachial nucleus, medial division
PCRt	parvocellular reticular nucleus
PCRtA	parvocellular reticular nucleus, alpha
PMn	paramedian reticular nucleus
PnC	pontine reticular nucleus, caudal part
PPy	parapyramidal nucleus
Pr	prepositus nucleus
Pr5DM	principal sensory trigeminal nucleus, dorsomedial part
Pr5VL	principal sensory trigeminal nucleus, ventrolateral part
py	pyramidal tract
RAmb	retroambiguus nucleus
RF	reticular formation (of medulla)
RMg	raphe magnus nucleus
Ro	nucleus of Roller
ROb	raphe obscurus nucleus
RPa	raphe pallidus nucleus
RVL	rostroventrolateral reticular nucleus
SO	superior olive
Sp5C	spinal trigeminal nucleus, caudal part
Sp5I	spinal trigeminal nucleus, interpolar part
Sp5OVL	spinal trigeminal nucleus, oral part
SpVe	spinal vestibular nucleus
Su5	supratrigeminal nucleus
T	solitary tract
T5	spinal trigeminal tract
VCP	ventral cochlear nucleus, posterior part
4V or IV	4th ventricle
5N	motor trigeminal nucleus
7N	facial nucleus
10N or X	vagal motor nucleus
12N or XII	hypoglossal nucleus
NST	*subnuclei*
Ce	central subnucleus
CL	caudal lateral subnucleus
COM	commissural subnucleus
DL	dorsal lateral subnucleus
M	medial subnucleus
PC	parvicellular subnucleus
RC	rostral central subnucleus
RL	rostral lateral subnucleus
RM	rostral medial subnucleus
V	ventral subnucleus
VL	ventral lateral subnucleus

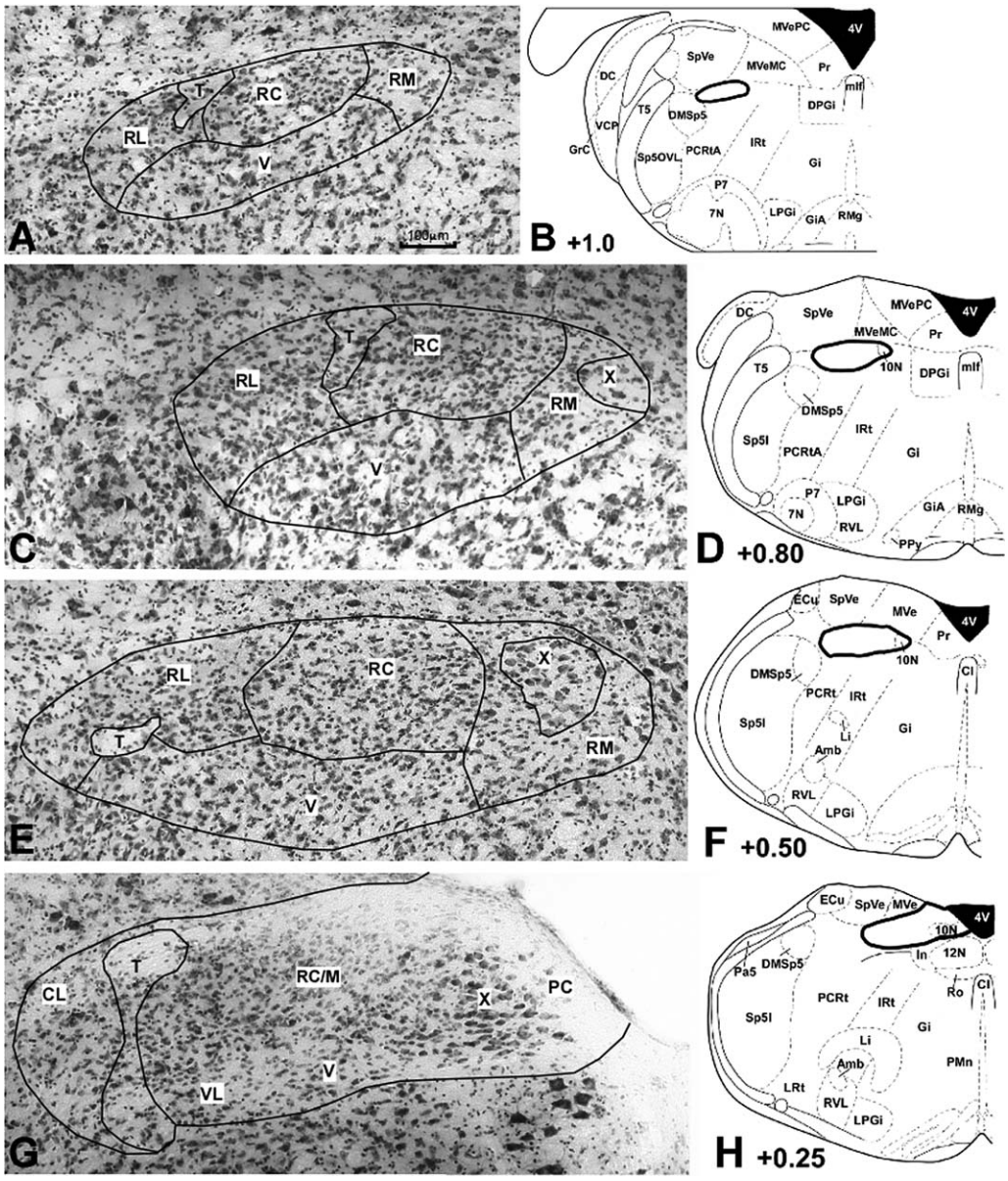

Figure 1. **A–P** are a representative rostrocaudal series of coronal, Nissl-stained sections through the NST in the C57BL/6J mouse. In this figure and Figures 6–12, 14, 16, 17 numbers adjacent the photomicrographic or schematic sections indicate the distance (mm) of each section from the obex (=0.0) as defined here (see Materials and Methods). A–F: Rostral division of NST. G,H: Rostralmost part of the intermediate division of NST. I,J: Transitional zone between caudal and intermediate divisions of NST. K–P: Caudal division of NST. Schematics accompanying each section are adapted from Paxinos and Franklin (2001) and indicate the location of NST (circumscribed with a continuous thick line) relative to other medullary structures. In all photomicrographs and schematics, dorsal is upward and lateral is to the left of the section. For abbreviations see list. Scale bars = 100 μm.

utilizing the anterograde and retrograde transport of cholera toxin subunit B (CTb; Luppi et al., 1990; Angelluci et al., 1996), several key connections were mapped in NST: 1) NST subnuclei receiving chorda tympani nerve (CT; innervating anterior tongue fungiform and anterior posterolateral tongue foliate taste buds) afferent endings; these results supplement the $P2X_2$ material; 2) NST subnuclei exhibiting efferent and afferent connections with the PBN; 3) the medullary RF; and 4) NST subnuclei that interconnect the rostral/intermediate and caudal divisions of the NST. Schematic illustrations summarizing CT (Whitehead and Frank, 1983; Fig. 1) and central gustatory structures (Whitehead and Finger, 2008, Fig. 14) examined in the present study have been described. This CTb analysis also reveals the brainstem source of presynaptic visceromotor (superior salivatory nucleus) efferents passing in the CT. A portion of these results has been previously reported (Bartel et al., 2007; Ganchrow et al., 2007).

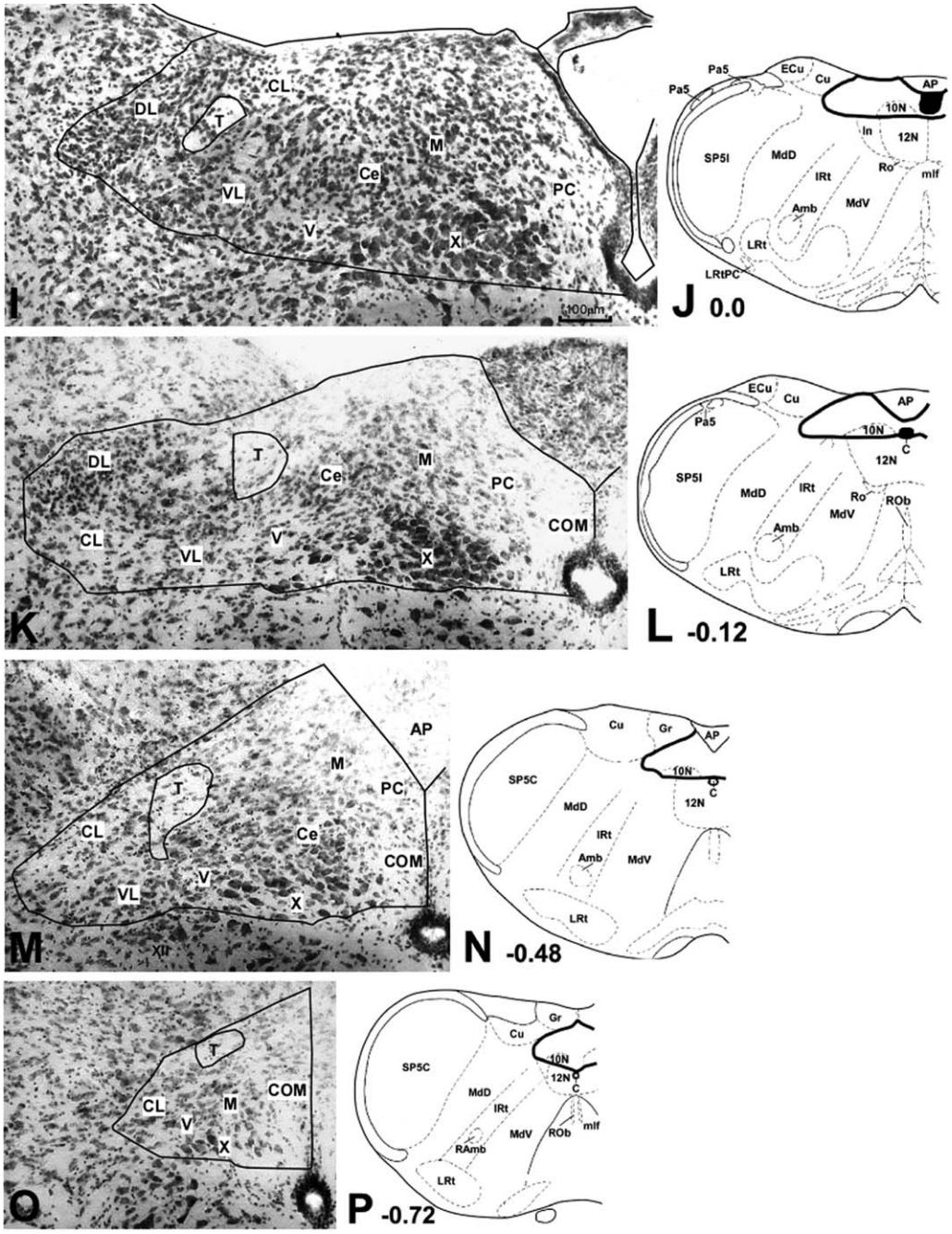

Figure 1. (Continued)

MATERIALS AND METHODS

Animals

Forty-four C57BL/6J mice, ages 6–20 weeks, of 20–40 g GBW were utilized in this study (Jackson Laboratory, Bar Harbor, ME). All laboratory procedures were approved by the University of California at San Diego Laboratory Animal Care and Use Committee and the University of Colorado Denver Anschutz Medical Campus Institutional Animal Care and Use Committee and followed the National Institutes of Health *Guide for the care and use of laboratory animals*. Five animals received CTb (highly purified B subunit isolated from *Vibrio cholerae* type Inaba 569B, product 103B; List Biological, Campbell, CA) injections into the CT in the middle ear; 11 animals received injections into the PBN; and 11 animals received injections into the medullary RF ventromedial to the rostral NST, the pontine RF, or the vestibular nuclear complex. Finally, for surveying intranuclear connections, eight animals received injections into the NST targeting either the rostral or the

caudal divisions (defined below). Two mice were utilized to prepare a cytoarchitectonic atlas based on routine Nissl staining (cresyl violet) of the NST. Four additional animals were utilized for reduced NADPH-diaphorase (Sigma-Aldrich, St. Louis, MO; catalog No. N5130) staining of the NST, according to the protocol of Gonzalez-Zulueta et al. (1999) and as previously described by Scherer-Singler et al. (1983). To optimize the view of NADPH staining along the rostral–caudal extent of the NST, the brains of two of these animals were sectioned in the horizontal plane. Cresyl violet-stained sections adjacent to the sections stained for NADPH aided in identifying NST subnuclei revealed with the latter stain (see for rat Herbert et al., 1990). Finally, medullary tissue from three animals was prepared for immunoreactivity (IR) for $P2X_2$, an ionotropic receptor for ATP that is expressed on taste cells (Hayato et al., 2007), on both primary afferent gustatory and primary afferent general viscerosensory nerve fiber membranes (Bo et al., 1999; Atkinson et al., 2000; Finger et al., 2005; Ishida et al., 2009) and on their terminals within the gustatoviscerosensory NST (Kanjhan et al., 1999; Yao et al., 2001; Bartel, 2012).

Surgery and CTb injections

Animals were initially calmed in a bell jar containing isoflurane vapors (Piramal Healthcare, Bethlehem, PA; lot No. A11D11A), then anesthetized with pentobarbital (45–70 mg/kg, i.p., Hospira, Lake Forest, IL; list No. 3778) and placed on a warming platform, and their heads were stabilized with a nose clamp and lower bar assembly that accommodates the upper incisors. CTb injections were administered through a glass micropipette (tip diameter 15–20 μm) attached to and advanced by a micromanipulator (Fine Science Tools, San Francisco, CA). In five animals, the CT was reached in a lateral approach to the middle ear by incising the tympanic membrane and pulling ventrally on the malleus, thereby exposing the nerve. The CT was slightly crimped with No. 5 surgical forceps to maximize anterograde transganglionic and retrograde transport of CTb via injury-filled fibers (see, e.g., Luppi et al., 1990), and 0.05 ml CTb (1mg/ml, suspended in sterile distilled water) and the label was ejected via the micropipette onto the nerve. Subsequently, the external auditory meatus was filled with surgical wax to maintain exposure of the CT to the CTb bathing the middle ear.

The PBN injections of CTb consisted of stabilizing the mouse's head by an approach described previously (Beckman and Whitehead, 1991). The occipital bone then was removed with rongeurs and the midline cerebellum aspirated to expose the dorsal surface of the medulla and caudal pons. The PBN was targeted visually, relative to the NST, based on surface features of the dorsolateral pons (for more detail see Whitehead, 1990). Six animals were injected using an iontophoretic pump (BAB-500; Kation Scientific, Minneapolis, MN) at a setting of 5 seconds on/5 seconds off (square anodal pulses), at 4 μA for 2–10 minutes. Five additional animals were PBN-injected using a Picospritzer (General Valve, Fairfield, NJ). These latter injections were made with 50 pulses at 9 msec each and 20 psi. For all PBN injections, micropipette tip diameters were 8–20 μm, and the 1 mg/ml CTb concentration was suspended in 16.5% methylene blue and 83.5% distilled water. In general, electrophoretic injections yielded smaller and denser injection sites, generating the cases depicted in the present article.

The RF was approached by surgically exposing the medulla as described above and targeting the rostral RF based on its location ventral and ventromedial to the rostral pole of NST. The latter reference point was localized based on its relationship to a consistent distinctive blood vessel on the dorsolateral surface of the medulla. In some cases, RF localization was aided further by using coordinates in the Paxinos and Franklin (2001) mouse atlas, i.e., measuring distances rostral to the visible AP and lateral to the midline. Rostral and caudal divisions of the NST were targeted as described above and also by reference to the AP. The AP was also injected. All CTb injections into RF and NST were iontophoretic, using the same pulse and timing parameters as with PBN iontophoretic injections.

Perfusion and tissue processing

Animals survived for 24–72 hours after CTb injections, after which they were anesthetized, the blood was flushed transcardially with phosphate-buffered saline (pH 7.4), and the animals were perfused transcardially with 4% paraformaldehyde in phosphate buffer (pH 7.4). The brain was blocked and the coronal plane established by a transverse cut through the midbrain perpendicular to rostral–caudal axis of the brain and to the surface on which its ventral aspect (consisting principally of the inferior temporal lobes and the pons) rests (with the spinal cord removed at the upper cervical level; Whitehead, 1988). The blocked tissue was transferred briefly into fresh perfusate and stored overnight in 40% sucrose. Coronal, 40-μm-thick sections between the high cervical spinal cord and midbrain inferior colliculus were cut on a freezing microtome (American Optical, Buffalo, NY).

Three animals that did not receive CTb injections were used for $P2X_2$ immunoreactivity. After perfusion, the brainstem was postfixed in 4% paraformaldehyde in phosphate buffer (pH 7.4) for 3 hours at room temperature. The tissue was then cryoprotected overnight with 20% sucrose in 0.1 M phosphate-buffered saline (PBS;

TABLE 1.
Antibody Characterization

Antibody	Immunogen	Host, type	Manufacturer	Dilution
Primary	Cholera toxin subunit B from *Vibrio cholerae*	Goat, polyclonal	List Biological, catalog No. 703	1:10,000
Secondary	Goat IgG	Rabbit, polyclonal	Vector, catalog No. BA-5000	1:200
Primary	$P2X_2$ Synthetic peptide to rat C-terminus (SQQDSTSTDPKGLAQL)	Rabbit, polyclonal	Alomone, product No. APR-003	1:500
Secondary	Rabbit IgG, Alexa 568	Goat, polyclonal	Invitrogen, catalog No. A11011	1:400

pH 7.4) at 4°C. On the next day, the brainstem was mounted in OCT compound (optimal cutting temperature; Fisher Scientific, Pittsburgh, PA), and 40-μm free-floating sections were cut on a cryostat.

CTb Immunocytochemistry

Free-floating tissue sections were reacted for the immunocytochemical demonstration of CTb using goat anti-CTb (List Biological Laboratories, catalog No. 703; 1:10,000) primary antibody overnight at 4°C on a rotating shaker. Bound antibody was revealed by reacting the free-floating sections with biotinylated rabbit anti-goat IgG (Vector, Burlingame, CA; catalog No. BA-5000; 1:200) secondary antibody for 1 hour, followed by reaction in 0.3% hydrogen peroxide and diaminobenzidine (MP Biomedicals, Solon, OH; catalog No. 98068) for 4 minutes. Rinses with phosphate-buffered saline (pH 7.4) separated each step of the immunocytochemical protocol. Sections were mounted on albumin-gelatin-coated slides and counterstained with either Giemsa (EMD Chemicals, Billerica, MA; catalog No. 620G-75; which darkens the CTb reaction product while rendering the cytoarchitecture visible) or cresyl violet (Chroma-Gesellschaft, Munich, Germany; catalog No. 1A396) for Nissl staining. In some cases, alternate sections were either solely CTb reacted or solely Nissl stained. Control tissue was immunonegative in cases in which CTb was not applied to the CT or injected intracranially.

$P2X_2$ immunocytochemistry

After three 10-minute washes in 0.1 M PBS (pH 7.4), the tissue sections were incubated in blocking solution (3% normal goat serum, 1% bovine serum albumin, 0.3% Triton in PBS) for 1 hour at room temperature. The sections were then incubated overnight at 4°C with the rabbit anti-$P2X_2$ primary antibody (Alomone, Jerusalem, Israel; catalog No. APR-003; 1:500). Sections were washed three times in PBS and incubated for 2 hours with Alexa 568 goat anti-rabbit secondary antibody (Invitrogen, Eugene, OR; catalog No. A11011; 1:400). After three 10-minute washes in PBS, the sections were rinsed in 0.1 M phosphate buffer and then incubated with green fluorescent Nissl fluorophore (Molecular Probes, Eugene, OR; catalog No. N-21480; 1:200) at room temperature for 20 minutes. The tissue sections were washed twice in phosphate buffer, mounted onto Superfrost Plus slides (Fisher Scientific, Pittsburgh, PA), and coverslipped with Fluoromount G (Southern Biotechnology Associates, Birmingham, AL).

$P2X_2$ antibody characterization

$P2X_2$ antibody was made in rabbits against a synthetic peptide to the C-terminal domain of the rat $P2X_2$ sequence (for more details regarding the antibody see Table 1). According to the manufacturer's technical information, a single band at 80 kD was detected on Western blots from PC12 lysates. This antibody has been verified by staining taste tissues from mice in which the $P2X_2$ receptor was genetically deleted; no signal was detected (Finger et al., 2005). In addition, this antibody has been characterized in the rostral medulla of C57BL/6J mice (Bartel, 2012). The $P2X_2$ staining in the current study, namely, reactivity localized to fiber regions within the NTS as well as a scattering of motor neurons in more ventral regions, is consistent with the staining pattern previously described (Bartel, 2012). Omission of the $P2X_2$ antibody resulted in no apparent fluorescent signal. This confirmed that the secondary signal normally results from binding to the primary antibody (data not shown).

Images were acquired with an Olympus Fluoview confocal laser scanning microscope and ×20 oil objective, 0.80 numerical aperture, or ×10 objective, 0.40 numerical aperture. For each image, the channels were collected sequentially with a single wavelength excitation and then merged to produce the composite double-label image. This prevents the issue of bleed-through as a result of side-band excitation of the fluorophores.

NST atlas

For preparing a cytoarchitectonic atlas of the NST, two control brains were perfused and sectioned similarly

to the CTb cases, and a caudorostral Nissl series covering the ~2 mm extent of the NST, from 1 mm caudal to 1 mm rostral to the obex, was stained with cresyl violet. To characterize the NST further, and for comparison with Nissl staining, four additional control animals were perfused and sectioned as described above for NADPH-diaphorase staining, two in the coronal plane, two in the horizontal plane. In the present report, "obex" is defined as that section that most closely indicates the transition from the central canal into the fourth ventricle. In most instances, the obex coincides with the rostral pole of the AP (see Contreras et al., 1982; Kalia and Sullivan, 1982; Herbert et al., 1990; Corson et al., 2012). Working independently under microscopic (Eclipse E800; Nikon, Melville, NY) observation and photomicrographic analysis, two of the present investigators parcellated the NST into subnuclei based on Nissl or NADPH staining intensity, cell packing density, shape and size of cells, neuropil features, and location relative to the solitary tract and surrounding brain nuclei. NST nomenclature is based, in part, on that described for hamster (Whitehead, 1988) and mouse (Paxinos and Franklin, 2001). Descriptions of viscerosensory NST subnuclei in mouse (Ramón y Cajal, 1972) and rat (Herbert et al., 1990) also informed the present investigation. Eight (of 31) representative sections in the caudorostral series were selected to prepare the atlas presented here. Original photomicrographic images have been adjusted for gamma (or contrast) and corrections made for evenness of background and color balance (Adobe Photoshop).

Statistical analysis

Cells in each NST subnucleus, and in the vagal motor nucleus, were measured in atlas sections with Image Pro Plus (version 5.1.0.2; Media Cybernetics, Silver Spring, MD). Measurements were obtained from digital photomicrographic images, acquired at ×100 magnification, that were enlarged on the computer monitor to ×800, with the subnucleus of interest positioned within the field of view of the computer monitor. A 10 × 10 grid of 100 squares, superimposed on the monitor's display was subsequently made visible. Twenty squares were randomly selected, and within each square only cells showing a nucleolus were measured. Squares selected for cell measurements were determined by a random number generator that derives sets of two digit integers from atmospheric noise (www.random.org). The first and second digits were used to identify the column and row of each square to be analyzed. If the square fell outside of the subnucleus of interest, the next integer in the randomly derived set was used until 20 squares within the subnucleus were obtained. Measurements of cell (somal) area (μm^2) and diameter were compiled over three or four sequential histological sections for each subnucleus of NST. Mean cell area ± SD was determined for a total of 868 cells in all NST subnuclei and the vagal motor nucleus. Preliminary analysis indicated that the variance of somal area across NST subnuclei was not homogeneous, so somal area was tested by a nonparametric Kruskal-Wallis ANOVA (Statext v1.0; www.statext.com). Least significant difference between mean ranks post hoc comparisons of somal area between subnuclei were applied following a significant ANOVA (Siegel and Castellan, 1988).

Subnuclear analysis of retrogradely labeled NST cells after CTb injections in the NST, AP, PBN, or medullary RF was carried out thus: single sections were sampled at atlas levels +1.0, +0.80, +0.50, +0.25, 0.0, −0.12, −0.48, and −0.72 (see Fig. 1), and cells were counted by an investigator blind to the nature of the injection site. Under microscopic observation at a magnification of ×400, for each section, the subnucleus of interest was positioned in the approximate center of the microscopic field by viewing through the left eyepiece. An ocular reticle that was prepositioned over the center of the field with one edge parallel to the medullary midline raphe was then viewed through the right eyepiece and focused. The reticle was viewed after centering the area of interest through the left eyepiece of the microscope to avoid bias in selecting cells to count. The number of retrogradely labeled cells as well as the total number of cells within that subnuclear field (3,600 μm^2) were counted. Generally, only cells with a visible nucleus that was unfilled by CTb reaction product were counted. Counts also included a very small minority of heavily labeled cells with indistinct nuclei but that displayed a full somal envelope with the label extending into at least two filled primary dendrites. These raw counts were converted into estimates of the true numbers of labeled and unlabeled cells by applying the Abercrombie equation (Abercrombie, 1946). This calculation takes into account diameter measurements from the unlabeled and labeled cells. In the present application, the measurements, obtained in Image Pro Plus (as described above), were derived from areal tracings of the somal outlines. To apply the Abercrombie equation to our data we made the assumption that that the profiles that we traced were near the midportion of the cells and that the cells were spherical. The same statistical tests applied in comparing somal area across NST subnuclei were used to compare the proportions of retrogradely labeled cells across subnuclei. Level of significance was set at $P \leq 0.05$. The degree of retrograde labeling of cells is plotted on drawings as a qualitative representation of the quantitative analysis summarized above. For plotting retrogradely labeled cells and anterograde labeling of endings, each triangle

represents the location of four cell bodies, and each dot represents the location of five endings (Figs. 6, 8, 10, 11, 14, 16, 17). In cases with NST or AP injections, the degree of labeling within each NST subnucleus or non-NST medullary nucleus was then calculated as a percentage of the total for each case and represented as different sized dots in Figure 13.

RESULTS

Atlas of NST subnuclei: Nissl cytoarchitecture

Figure 1A–P presents a rostrocaudal series of coronal sections through the NST in the C57BL/6J mouse. High-magnification photomicrographs are of Nissl-stained sections through the NST in a representative intact case. Each photomicrograph is accompanied by a lower magnification schematic section at the same level, adapted from Paxinos and Franklin (2001), showing the topographic relation of the NST to surrounding medullary structures. Numbers accompanying each photomicrograph/schematic pair indicate distances (mm) from the obex [(0.0), as defined here; see Materials and Methods] in the fixed and sectioned brain.

The mouse NST extends the length of the medulla. It begins rostrally in the dorsolateral medulla at the level of the cochlear nuclei, immediately ventral to the vestibular nuclei, where the NST indents the medial spinal trigeminal nucleus (Fig. 1A,B). The NST extends caudally with a medial inclination to meet, first, the lateral border of the fourth ventricle (Fig. 1G,H), then, subsequently, the contralateral NST, the caudal poles of the NST merging at the midline beneath the AP and nucleus gracilis (Fig. 1K–P). The NST is oval in transverse section at rostral and intermediate rostrocaudal levels; it becomes triangular in cross section caudally. The nucleus is distinguishable by its mostly smaller and more densely packed neurons compared with non-NST neurons in the immediately surrounding areas of the medulla. Moreover, the paucity of myelinated axons in the NST renders it readily identifiable with phase microscopy in unstained sections of the medulla (data not shown; see also Whitehead, 1988). Within the NST, groups of neurons exhibit differences in somal area, packing density, or staining intensity that are guides to parcelling the nucleus into subnuclei by inspection. The range of somal areas in subnuclei of the NST, and in the vagal motor nucleus, is shown in Figure 2.

For the purpose of dividing the NST cytoarchitectonically into its component subnuclei, we defined three major divisions of the NST. The *rostral* division of the NST is here defined as beginning at its rostral pole (+1.0, with reference to the obex; Fig. 1A,B) and extending caudally for a distance of 0.7 mm, to +0.3, that level at which the nucleus shifts medially, approaching close to and nearly abutting the fourth ventricle. The *intermediate* division begins with the level at which the nucleus first borders the fourth ventricle (+0.25; Fig. 1G,H) and continues caudally to the obex (0.0; Fig. 1I,J). The *caudal* division of the NST continues caudally from the obex and merges with the contralateral NST below the AP, the caudal pole of NST (−1.0) lying above the central canal (Fig. 1O,P). These three regional divisions do not have abrupt cytoarchitectonic borders but, rather, successively transition one into the other (Fig. 1). Specifically for the rostral division (Fig. 1A,C,E), cytoarchitecture and CT projection data to the NST in mouse informed the outlined bordering of NST subnuclei. Subnuclear cytoarchitecture in intermediate and caudal divisions (Fig. 1G,I,K,M,O) of the NST is presented without outlined borders.

Rostral division of the NST

The *rostral central* (RC) subnucleus (Fig. 1A,C,E,G) extends for 0.75 mm, throughout the rostral division of the NST, and is transitional with the medial (M) subnucleus (see below) in the intermediate division of NST at +0.25 (Fig. 1G). RC lies medial to the solitary tract and directly ventral to the vestibular nuclear complex that occupies the dorsolateral medulla at rostral levels. RC is characterized by a dense collection of small to medium-sized neurons (mean cell area = 76.2 ± 16.8 [SD] μm^2, n = 60 cells; Fig. 2) that are distinctly smaller than those characterizing the dorsally adjacent vestibular complex.

The *rostral lateral* (RL) subnucleus (Fig. 1A,C,E) is located in the rostralmost ~0.70 mm of NST, lateral to RC, and is topographically continuous with the caudal lateral (CL) subnucleus (see below) in the intermediate division of the NST (Fig. 1G). In the rostralmost 0.2 mm of the NST, the solitary tract insinuates incompletely between RL laterally and RC medially. RL is characterized by small and medium-sized neurons (mean cell area = 81.1 ± 23.0 μm^2, n = 60 cells; Fig. 2), more loosely distributed than those of RC.

The *rostral medial* (RM) subnucleus (Fig. 1A–C,E) occupies the medialmost region of the NST and is characterized by a sparse concentration of cells. Somata are heterogeneous in size, i.e., relatively small-diameter cells staining lightly for Nissl substance, medium-sized cells, and some few neurons with large cell bodies (mean cell area = 92.1 ± 38.5 μm^2, n = 61 cells). Rostral to the obex, larger, more darkly staining cells of the rostral vagal motor nucleus (X) are embedded within RM (Fig. 1C,E). The dorsal motor nucleus of the vagus, although not a subnucleus of the NST, is outlined in

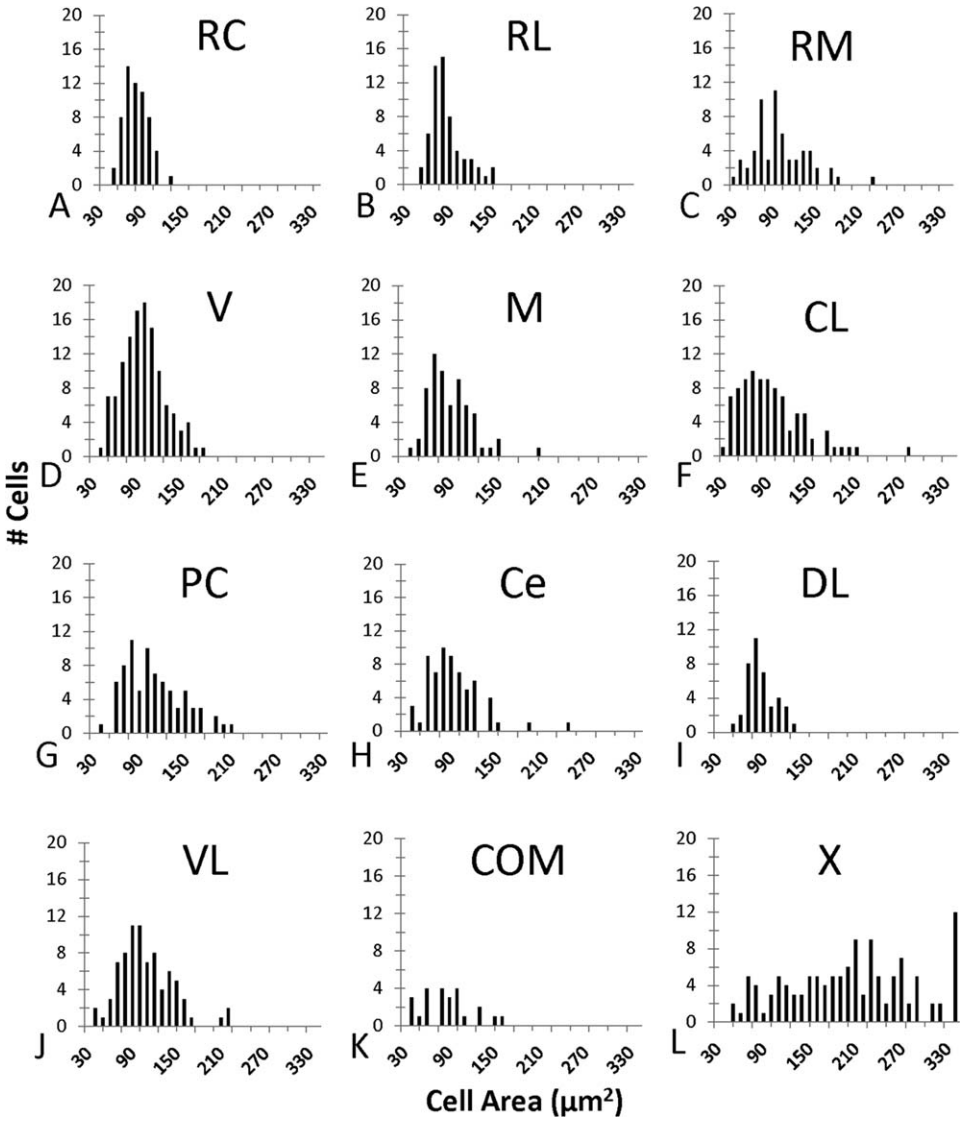

Figure 2. Histograms illustrating the frequency distributions of somal areas (μm^2) of cells measured in subnuclei of the murine NST and in the vagal motor nucleus. All of the subnuclei sampled overlap in areal measurements of small cells. However, the ventral subnuclei (V and VL) and the parvicellular (PC) subnucleus contain populations of larger cells not seen in RC, RL, DL, and COM, the latter four subnuclei distinguished by cells of relatively uniform small to medium size. The vagal motor nucleus (X) has the largest cells. For abbreviations see list.

Figure 1 and subsequent figures. RM is topographically continuous with the parvicellular (PC) subnucleus (see below) in the intermediate division of the NST (Fig. 1G).

The *ventral* (V) subnucleus occupies the ventral half of the NST in the rostral and intermediate divisions (Fig. 1A,C,E,G,I) and continues caudally throughout the caudal division of the NST (Fig. 1K,M,O; see below). V is characterized by loosely distributed cells, some of which are larger (mean cell area = 93.8 ± 28.9 μm^2, n = 120 cells; Fig. 2) than any in the immediately dorsal RC subnucleus. V directly overlies the medullary RF, a region with even larger and more widely spaced neurons with a distinct multipolar morphology.

Intermediate division of the NST

The *medial* (M) subnucleus (Fig. 1G,I,K,M,O) is topographically continuous with RC, occupying ~1.22 mm in the intermediate and caudal divisions of the NST. M is characterized by an overall denser cellularity than the surrounding subnuclei and consists of predominantly small to medium-sized neurons. Specifically, M is distinguished by a collection of relatively larger neurons (mean cell area = 84.5 ± 27.2 μm^2, n = 65 cells; Fig. 2) than in RC.

The *caudal lateral* (CL) subnucleus (Fig. 1G,I,K,M,O) is topographically continuous with RL in the intermediate division and continues caudally throughout the caudal

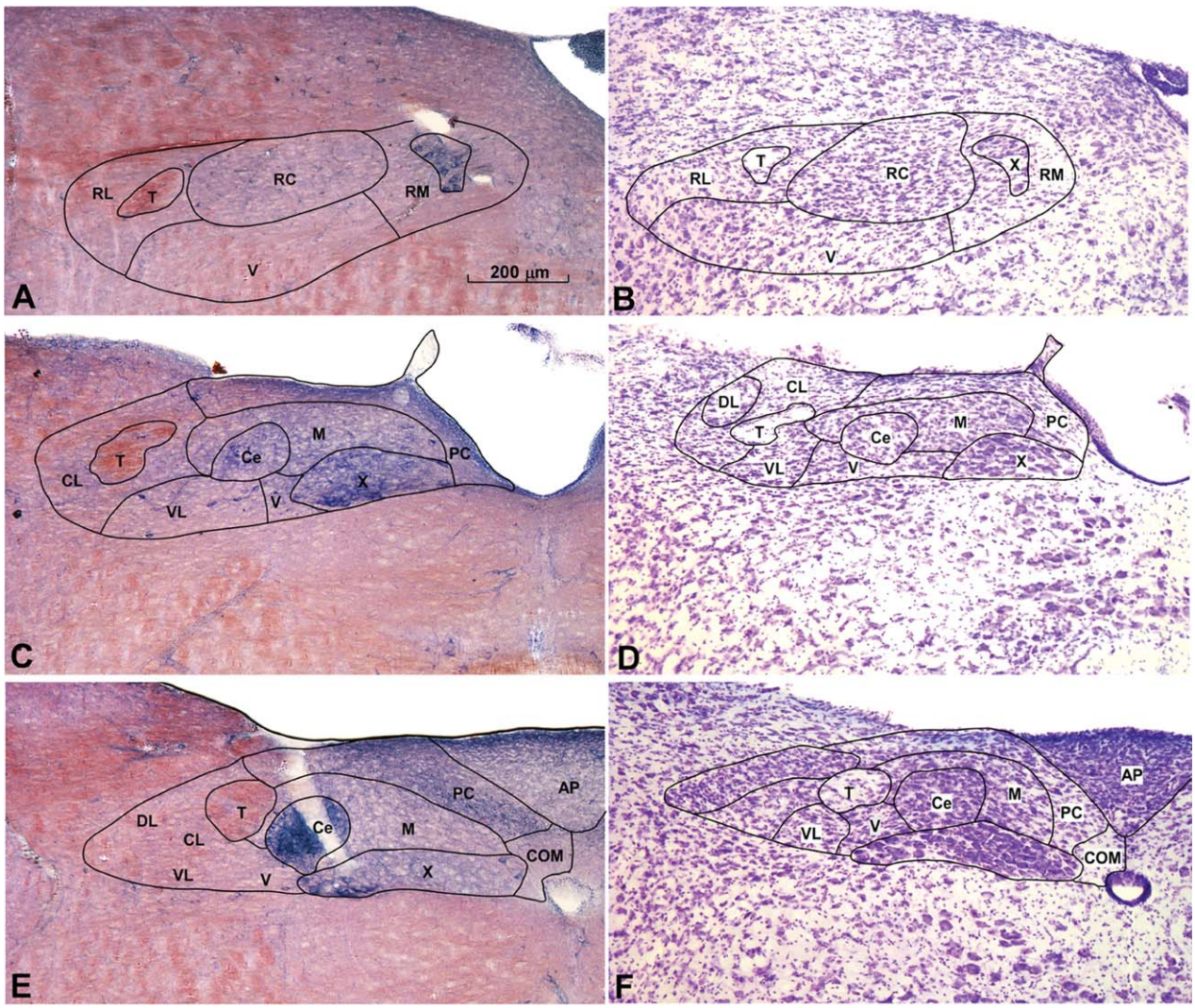

Figure 3. Coronal sections through rostral (**A,B**) and caudal (**C–F**) divisions of NST showing the differential staining of subnuclei with NADPH-diaphorase. Nissl-stained sections (B,D,F) are immediately adjacent to NADPH-diaphorase stained sections (A,C,E). In caudal NST at −0.48 (E,F), and the transition zone between caudal and intermediate divisions of NST at +0.05 (C,D) relative to the obex (0.0), particularly intense, deep-blue NADPH-diaphorase staining is evident within neuropil of Ce subnucleus. In rostral NST at +0.80 (A,B) relative to the obex, RC subnucleus exhibits moderate NADPH-diaphorase staining. Qualitatively moderate NADPH-diaphorase staining is seen in PC and M in C,E. For abbreviations see list. Scale bar = 200 μm.

division of the NST, lying lateral to the solitary tract. CL is characterized by a less dense arrangement of cells than M subnucleus, which medially abuts the former. CL is distinguished from RL by a broader distribution of somal sizes, including some larger cells (mean cell area = 90.2 ± 44.3 μm^2,n = 91 cells; Fig. 2).

The *parvicellular* (PC; Fig. 1G,I,K,M) subnucleus is topographically continuous with RM subnucleus and lies medial to the vagal motor nucleus (V; see below) in the intermediate division of the NST. PC continues caudally into the caudal division of the NST, where it lies between the M and commissural (COM, see below) subnuclei at the level of the AP. PC is characterized primarily by a loose collection of pale-staining neurons (mean cell area = 103.8 ± 37.0 μm^2, n = 78 cells). Sometimes PC neuropil exhibits moderate NADPH-diaphorase staining but qualitatively less intensely than the RC or Ce subnuclei (see below; Fig. 3; see also for rat Herbert et al., 1990, Fig. 1, p. 544; Broussard et al., 1995).

Caudal division of the NST

The *central* (Ce) subnucleus, lying ventrolateral to M subnucleus, is a restricted, especially densicellular, round region with relatively darkly staining, round somata in Nissl material (Figs. 1I,K,M, 3D,F). The cells

vary in size but are predominantly medium sized (mean cell area = 87.3 ± 34.1 μm^2, n = 65 cells). At the rostral AP/obex level, the maximum width of Ce is ~200 μm (Figs. 1I, 3C–F, 4B). At this level and extending caudally, Ce is characterized by a distinctive, relatively more intense NADPH-diaphorase staining of its neuropil compared with surrounding NST subnuclei (Figs. 3C,E, 4A) At the obex level and caudally, Ce also is characterized by relatively intense $P2X_2$ IR in preterminal axons and in endings (varicosities; Fig. 5). Some of these endings appear to arise from probable vagal nerve, $P2X_2$-immunopositive afferents in the solitary tract (Fig. 5A, inset).

The *dorsal lateral* (DL) subnucleus (Fig. 1I–K) is topographically continuous with CL and is present primarily at the level of the obex, extending ~0.12 mm caudal to the obex. DL is distinctively elongated; is oriented dorsomedially to ventrolaterally; and contains densely packed, darkly stained somata. DL is further characterized by a narrow distribution of small to medium-sized neurons (mean cell area = 82.4 ± 18.5 μm^2, n = 40 cells; Fig. 2).

The *ventral lateral* (VL) subnucleus (Fig. 1G–N) extends ~0.73 mm in the NST, with its greater portion lying caudal to the obex. VL neurons are moderately concentrated, and more darkly staining than cells in the V subnucleus. VL further is characterized by a small but distinct subset of the largest neurons of the NST, contributing to a relatively large average cell body diameter (mean cell area = 103.5 ± 36.8 μm^2, n = 80 cells; Fig. 2).

The *ventral* subnucleus (V), present in the rostral and intermediate divisions of NST also extends into the caudal division of NST. In the caudal NST, V occupies the greater portion of the ventral sector of the NST, ventral to M and Ce, medial to VL, and ventromedial to CL subnuclei. V tapers in size caudally and ends just before the caudalmost pole of the NST (Fig. 1K,M,O).

The *commissural* (COM) subnucleus (Fig. 1F–H), initially described for the mouse by Ramón y Cajal (1972), extends caudally from the obex, initially lying ventromedial to the PC subnucleus of the NST, and medial and dorsomedial to the distinctively larger, darker staining cells of the vagal motor (X) and hypoglossal (XII) nuclei. In the C57BL/6J mouse at the level of the AP, and in keeping with Ramón y Cajal's description, COM extends dorsally from the central canal to the base of the AP and medially to the midline. COM contains relatively small (mean cell area = 82.1 ± 33.3 μm^2, n = 24 cells) cells as well as cell-sparse regions of neuropil above the central canal (Fig. 1F–H) through which COM fibers cross the midline to terminate in contralateral COM (Ramón y Cajal, 1972, Fig. 306, Golgi preparation,

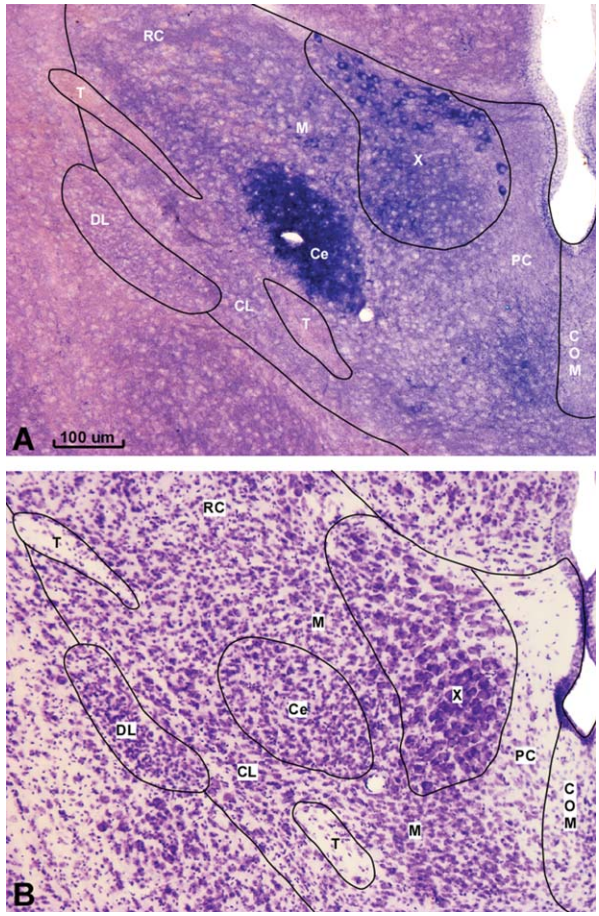

Figure 4. NADPH-diaphorase staining of NST subnuclei in a horizontal section (**A**). The adjacent section is Nissl stained (**B**). Intense staining highlights the Ce subnucleus and motor X nucleus. Less intense NADPH-diaphorase staining is present in M and RC subnuclei. The solitary tract is devoid of staining. For abbreviations see list. Scale bar = 100 μm.

p. 738). There is sometimes not a clearcut separation between the ventralmost cells of COM and similarly sized cells lying, respectively, medial and dorsomedial to X and XII nuclei. These small cells appear to be a medial extension of the intercalated nucleus.

Kruskal-Wallis ANOVA of somal area (rf. Fig. 2) across NST subnuclei is significant (H = 48.8, df = 10, $P \leq 0.05$). Post hoc comparisons indicate that the somal area of RC is significantly ($P \leq 0.05$) smaller than that of V, VL, and PC subnuclei. Additionally, RL somal area is significantly smaller than that of VL and PC subnuclei, and M area is smaller than that of VL ($P \leq 0.05$).

The larger somata of the vagal motor nucleus (X; mean cell area = 203.5 ± 91.6 μm^2, n = 124 cells) serve as a distinct referent in contrast to the surrounding smaller cells of the NST, from +0.8 to the caudal pole of the NST (Fig. 1C,E,G,I,K,M,O). At levels +0.5 to

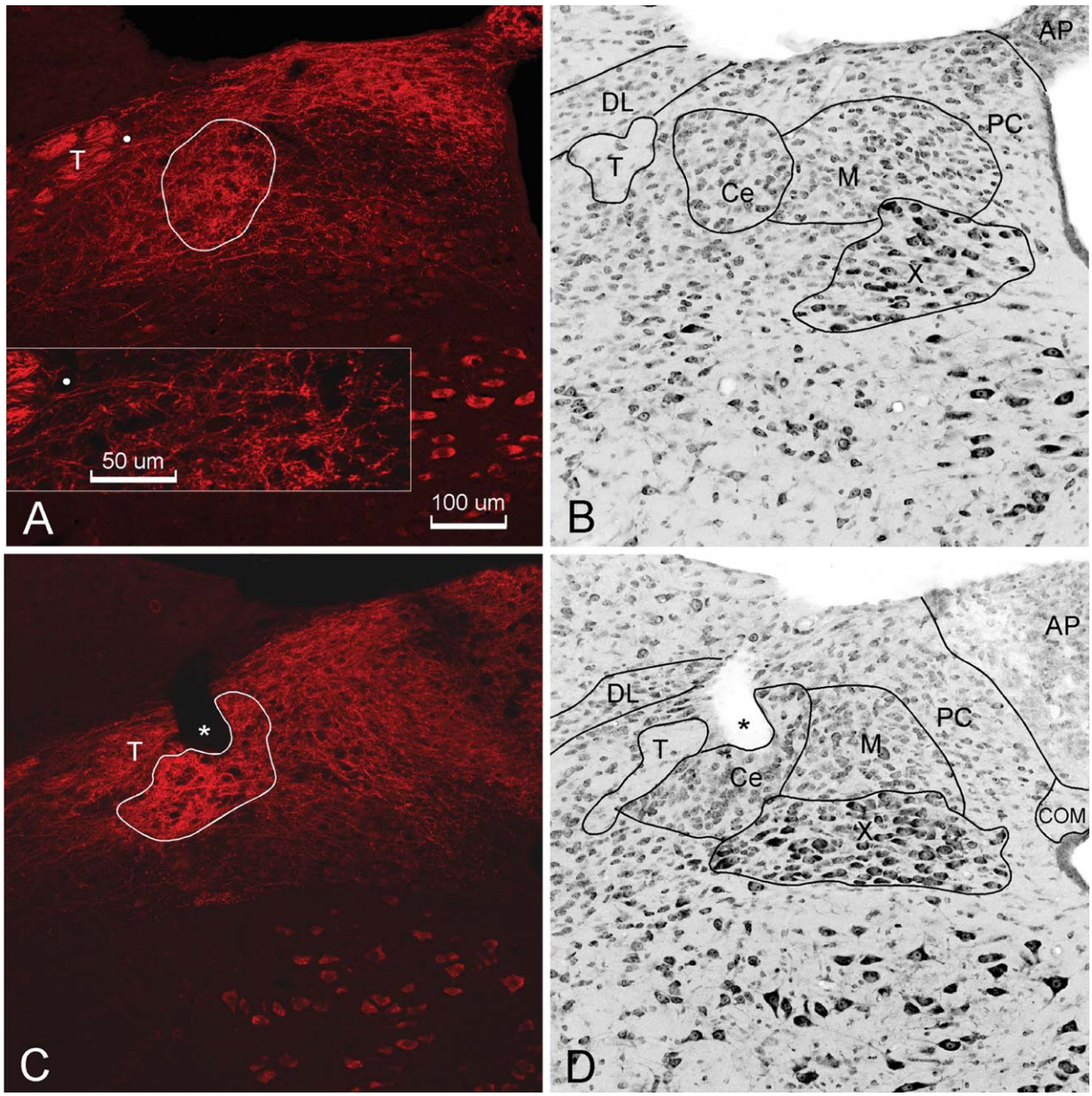

Figure 5. Confocal images of $P2X_2$-IR in the caudal NST at the level of the area postrema, approximately +0.06 (**A,B**) and −0.18 (**C,D**) relative to the obex. A,B and C,D are the same sections immunolabeled for $P2X_2$ (red channel) and Nissl fluorescence. NST cytoarchitecture as seen in B,D was achieved by successively converting the Nissl fluorophore channel to gray scale and inverting in Photoshop. A,C show $P2X_2$-IR (red) localized within solitary tract (T) fibers of probable vagal nerve origin at these caudal levels. The white dot in A indicates the location of the **inset** at higher magnification showing $P2X_2$-immunopositive solitary tract fibers directly entering Ce (white outline) and exhibiting particularly intense $P2X_2$-IR in preterminal axons and in endings (varicosities) within Ce. Also note that DL and X are relatively $P2X_2$ immunonegative. An asterisk indicates the same blood vessel in C,D. For abbreviations see list. Scale bars in A = 100 μm in A-D; 50 μm in inset.

+0.8, X cells lie embedded within the RM subnucleus of NST (Fig. 1C,E). These rostralmost large, darkly stained cells embedded within RM resemble in size and staining intensity those definitively identified as X farther caudally. Furthermore, they are distinguished from cells of the superior salivatory nucleus; the latter, retrogradely labeled by application of CTb to the chorda tympani, are located rostroventral to the NST (see below; cf. for rat: Contreras et al., 1980, Fig. 4, p. 380 and Fig. 10, p. 390; for hamster Whitehead and Frank, 1983, Fig. 2, p. 382). However, we cannot rule out the possibility that some cells in X at rostral NST levels include inferior salivatory nucleus neurons some of which, in the rat, lie within or medially adjacent the

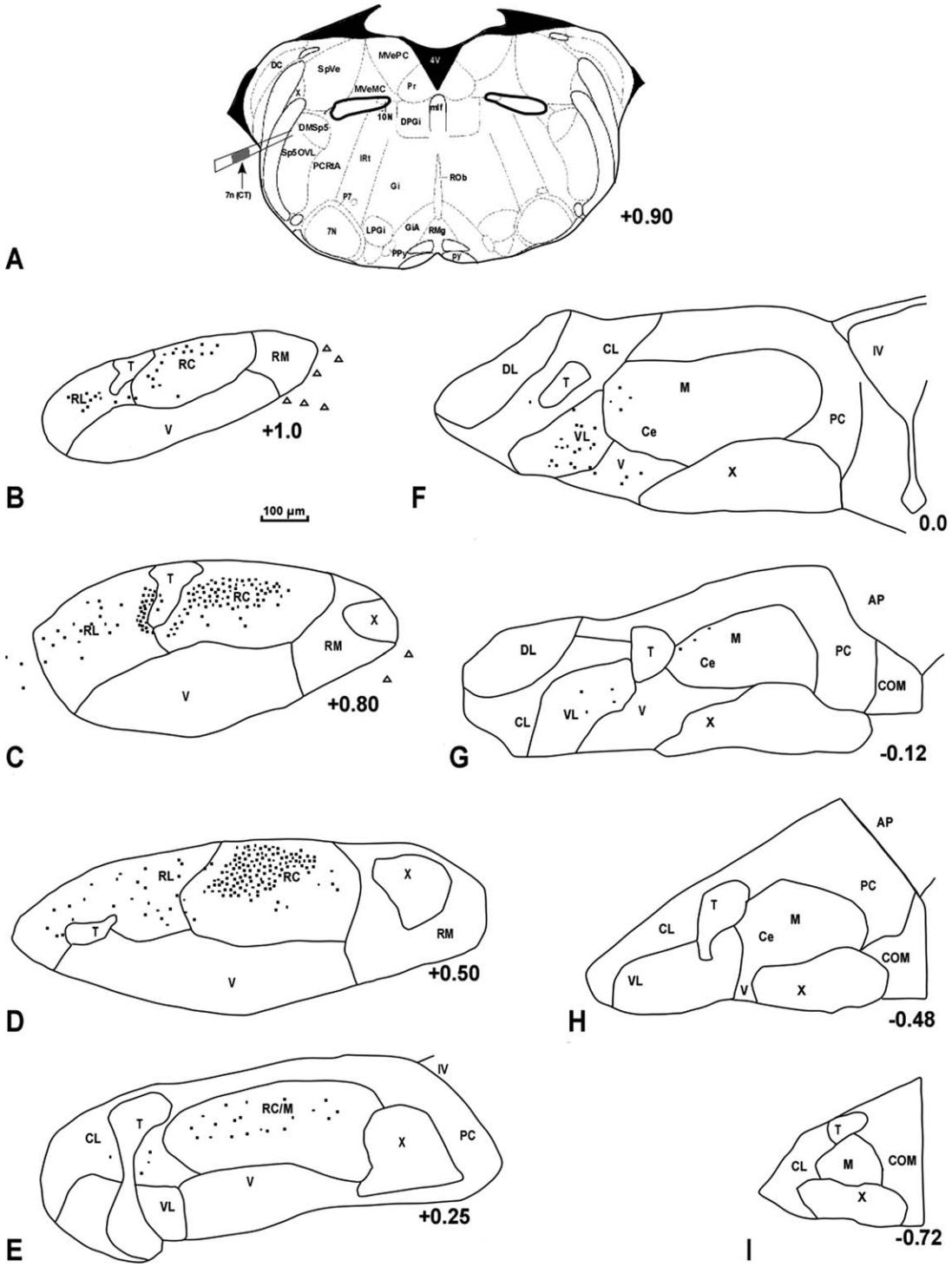

Figure 6. **A–I**: Qualitative plots of the relative density of CTb-labeled endings (dots) in the NST after chorda tympani nerve (CT, arrow, uppermost schematic) labeling. The schematic in this and the subsequent figures of plotted label are adapted from Paxinos and Franklin (2001). Primary afferent endings in the NST are concentrated at rostral levels in the dorsal half of RC. Sparser distributions are present in RL of the rostral division of the NST, i.e., at +1.0, +0.8, and +0.5 relative to the obex, and in the intermediate and caudal divisions in M, VL, V, and CL. Single, retrogradely labeled cells (triangles) of the superior salivatory nucleus lie medioventral to the RM subnucleus of the NST, at +0.8 to +1.0 rostral to the obex; their numbers as shown are a qualitative estimate. For abbreviations see list. Scale bar = 100 µm.

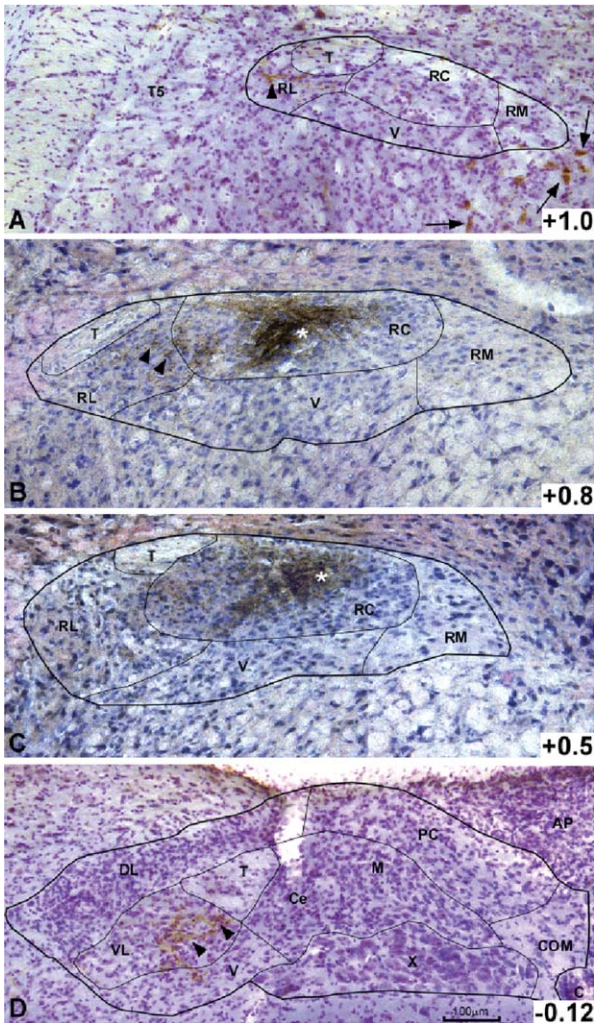

Figure 7. Terminal projection field endings (black/brown) of the chorda tympani, after labeling with CTb, are concentrated in the rostral NST (**A–C**); same case as plotted in Figure 6. Photomicrographs show that endings are most dense in RC (asterisks in B,C), less so in RL (arrowheads in A,B), and absent in other NST subnuclei. Caudal to the obex (**D**), some endings reach VL (arrowheads). Arrows in A show the preganglionic somata of the superior salivatory nucleus labeled by retrograde transport of CTb. For abbreviations see list. Scale bar = 100 μm.

medial portion of the rostral NST (cf. for rat: Contreras et al., 1980, Fig. 8, p. 386, and Fig. 10, p. 390; Kim et al., 2004, Figs. 1 and 2, pp. 29–30; Rezek et al., 2008, Figs. 2, 3, pp. 267–268).

NST subnuclei: NADPH staining and $P2X_2$ immunoreactivity

NADPH histochemistry specifically stains subregions of the NST and is virtually absent from most of the immediately surrounding brainstem nuclei. The specific pattern of NADPH staining in the mouse supports the present parcellation of the NST into subnuclei; some subnuclei are stained, staining that follows the same boundaries as in the Nissl material, and other subnuclei are unstained. NST NADPH staining was evident in the rostral division, where it lightly but distinctly stains the neuropil of the RC subnucleus and, to a lesser extent, the RM subnucleus (Fig. 3A,B). Other subnuclei rostrally are unstained. Motor X cells are intensely stained. In the caudal division, NADPH staining is generally more intense, with light staining in M, moderate staining in PC, and intense staining that precisely delineates Ce. DL, CL, and COM are very lightly stained; VL and V are mostly unstained (Fig. 3C–E). Apart from the NST, the AP stains moderately. Motor X, as in the rostral division, stains intensely.

In horizontal sections through the dorsal half of the NST, the size, shape, and extent of the nuclear complex are evident by its differential staining. Ce, in particular, presents as an intensely stained oval cell group that bridges the intermediate and caudal divisions (Fig. 4A). The horizontal view also shows the consistency and coextensiveness of light NADPH staining of RC and M. As in the transverse sections, PC exhibits moderate staining; COM, DL, and CL exhibit faint staining; and the solitary tract is clearly evident by its absence of stain.

In addition to intense $P2X_2$ IR within the Ce subnucleus (see above under Caudal division of the NST), moderate $P2X_2$ fiber IR coincides with the PC subnucleus. Subnucleus M is lightly populated with $P2X_2$-immunopositive fibers. Motor X contains rare $P2X_2$ fibers; motor XII contains none (Fig. 5).

Chorda tympani projections to the NST

Figures 6 and 7 are representative cases summarizing data in those animals ($n = 5$) receiving CTb injections of the CT nerve in the middle ear. In Figure 6, the relative distribution of CTb-labeled, terminal projection field endings is plotted qualitatively as dots throughout the rostrocaudal extent of the NST. Primary afferent endings extend for ~1.12 mm in the NST and are concentrated mainly at levels rostral to and including the obex; in the rostralmost 0.50 mm (i.e., rostral division) of the NST, the dorsal half of the RC subnucleus receives the densest degree, and the RL subnucleus a relatively sparser distribution of anterior tongue taste afferent inputs. CTb-labeled axons are typically seen as smooth and are lightly labeled in the present material (not illustrated), and presumed terminals are seen as ovoid swellings on or distributed among the axons and display a distinctly dense, punctate appearance (Fig. 7A–C). In the intermediate and caudal divisions, additional sparse endings are seen in M, VL, V, and CL subnuclei, with the caudalmost terminal projection field

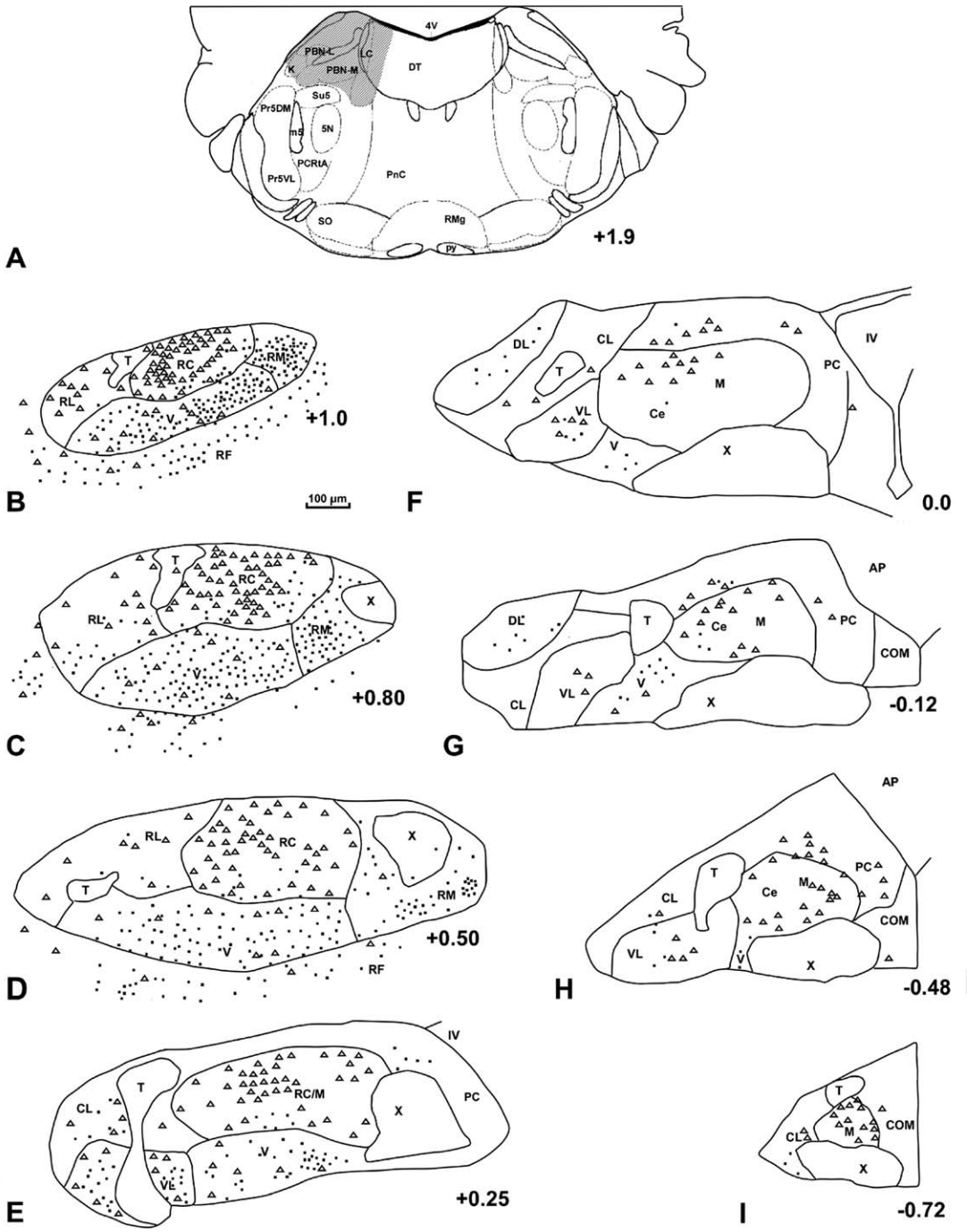

Figure 8. **A–I**: Qualitative plots of retrogradely labeled NST projection cells to the PBN (triangles), and the PBN projection field in NST and RF (dots), after CTb injection (diagonal lines, uppermost schematic) into the PBN proper. The injection site extends laterally to include the medial portion of the Kölliker-Fuse nucleus (K), and medially into the locus ceruleus (LC) and the dorsolateral tegmentum (DT). NST-PBN projection cells are located mainly in RC and M and are less concentrated in V and RL, with the fewest projection cells seen in VL, RM, and CL. Rostral to the obex, terminal projection field endings in NST predominate in the V and RM subnuclei and in the RF immediately subjacent to the NST. Rostral and caudal to the obex, sparser endings are seen in RL, DL, CL, and VL, including minor projections to the ventral sector of RC and M in the NST. For abbreviations see list. Scale bar = 100 μm.

evident at 0.12 mm below the obex level (Figs. 6, 7D, arrowheads). In addition, at the rostralmost level of the NST (+1.0, +0.8), CTb-labeled somata of the superior salivatory nucleus are seen, lying immediately medioventral to the RM subnucleus of the NST (Figs. 6, 7A). This latter labeling results from retrograde transport of CTb within distally projecting preganglionic parasympathetic fibers that contribute to the CT.

NST-PBN connections

Analysis of 11 cases in which the dorsolateral pons was targeted for CTb labeling shows that eight mice had partial or complete injections into the PBN complex. Results in cases with retrograde and anterograde labeling in the NST and subjacent RF after partial PBN injections are consistent with those in which PBN was essentially completely injected. Figure 8 shows results in a case in which the PBN proper was CTb injected. The rostrocaudal extent of the injection is 1.2 mm. The uppermost schematic in Figure 8 also indicates that the injection extends laterally to include the medial portion of Kölliker-Fuse nucleus and medially into the locus ceruleus and the dorsolateral tegmentum, including the pontine RF. Though large, the injection site spares the rostral- and caudolateralmost parts of the lateral division of the PBN (data not shown). As qualitatively plotted in Figure 8, throughout the 1.72 mm rostrocaudal extent of the NST, RC and M show the densest concentration of retrogradely labeled somata (Fig. 8, triangles). In general, the distribution of retrogradely labeled cells throughout RC and M is not limited to particular regions and therefore differs from the dense target of chorda tympani preterminals and endings within the dorsal halves of RC and M (cf. Figs. 6, 7). Compared with RC and M, relatively fewer retrogradely labeled somata are evident in V and RL, with the fewest labeled somata seen in the RL, PC, CL, and RM subnuclei of the NST (Figs. 8, 9); Ce, COM, and DL somata are essentially unlabeled. ANOVA of the proportion of retrogradely labeled cells ($n = 342$ total cells, labeled and unlabeled) sampled across NST subnuclei is significant ($H = 32.117$, $df = 9$, $P \leq 0.05$). Among the retrogradely labeled cells sampled, 53% (37 of 69 neurons) are identified in RC and M.

Large CTb injections into the PBN also reveal terminal projections within the NST. In the rostralmost 0.75 mm (i.e., rostral and anterior intermediate divisions) of the NST, projections from the PBN and pontine RF form endings that predominate in V and RM subnuclei (Figs. 8, dots; 9A,B) and extend heavily into the RF immediately subjacent to the NST. Rostral and caudal to the obex in the NST, sparser endings are evident in the RL, CL, DL, and VL subnuclei; minor projections also are seen in the ventral sector of RC and M (Fig. 8).

Retrograde labeling in the NST after a small CTb injection into a lateroventral sector of the medial parabrachial nuclei (Fig. 10) is generally consistent with that following an injection into the larger PBN proper (Fig. 8). The uppermost schematic in Figure 10 shows that the injection extends medioventrally to include the lateral dorsal tegmental nucleus, locus ceruleus, and medial vestibular nucleus (connections related to these latter sites are not presented). The injection extends 0.6 mm rostrocaudally. As qualitatively plotted (Fig. 10, triangles), retrogradely labeled somata are identified mainly in RC and M, with fewer cells in the ventral (V

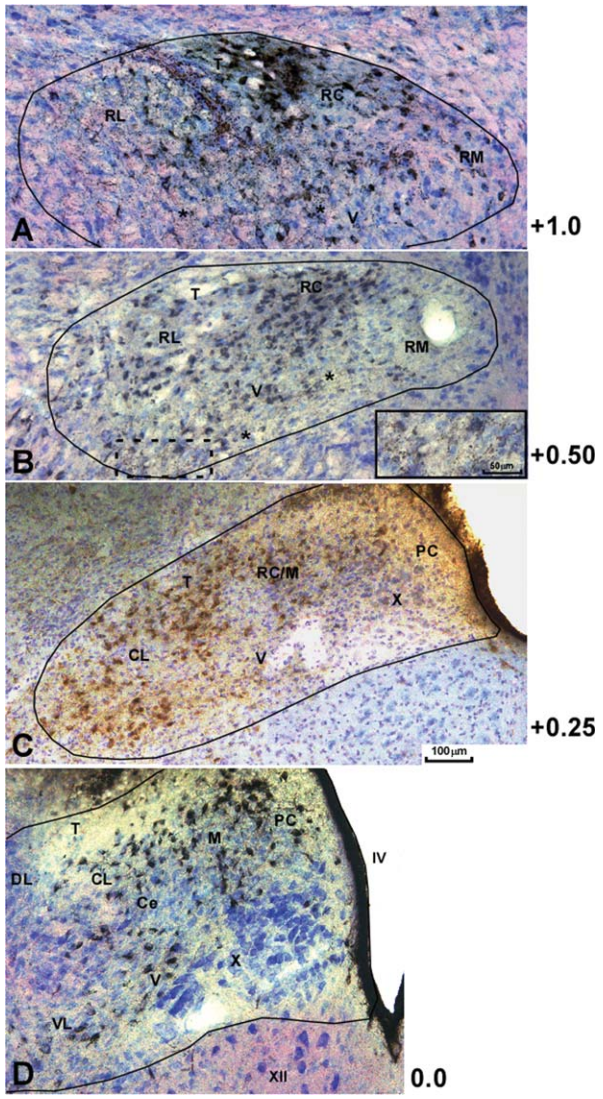

Figure 9. Photomicrographs of retrogradely labeled NST somata, and projection field terminations in the NST (outlined) after a large CTb injection of the PBN proper (Fig. 8, uppermost schematic); same case as plotted in Figure 8. In the rostral and intermediate divisions (**A–C**) and continuing caudally to the transitional zone between caudal and intermediate divisions of NST at the obex (**D**), retrogradely labeled cells are densely concentrated in RC and M and, as seen here, are qualitatively fewer in RL, CL, VL, V, and RM. Labeled terminal projection field endings (asterisks in A,B) in the rostral NST predominate in subnucleus V (see higher magnification **inset** in B). Sections A,B,C,D were Nissl counterstained with cresyl violet or Giesma. The Giesma stain renders the CTb reaction product black. Sections depicted are from the same or adjacent sections as those in Figure 8. For abbreviations see list. Scale bars in C = 100 µm in A-D; 50 µm in inset.

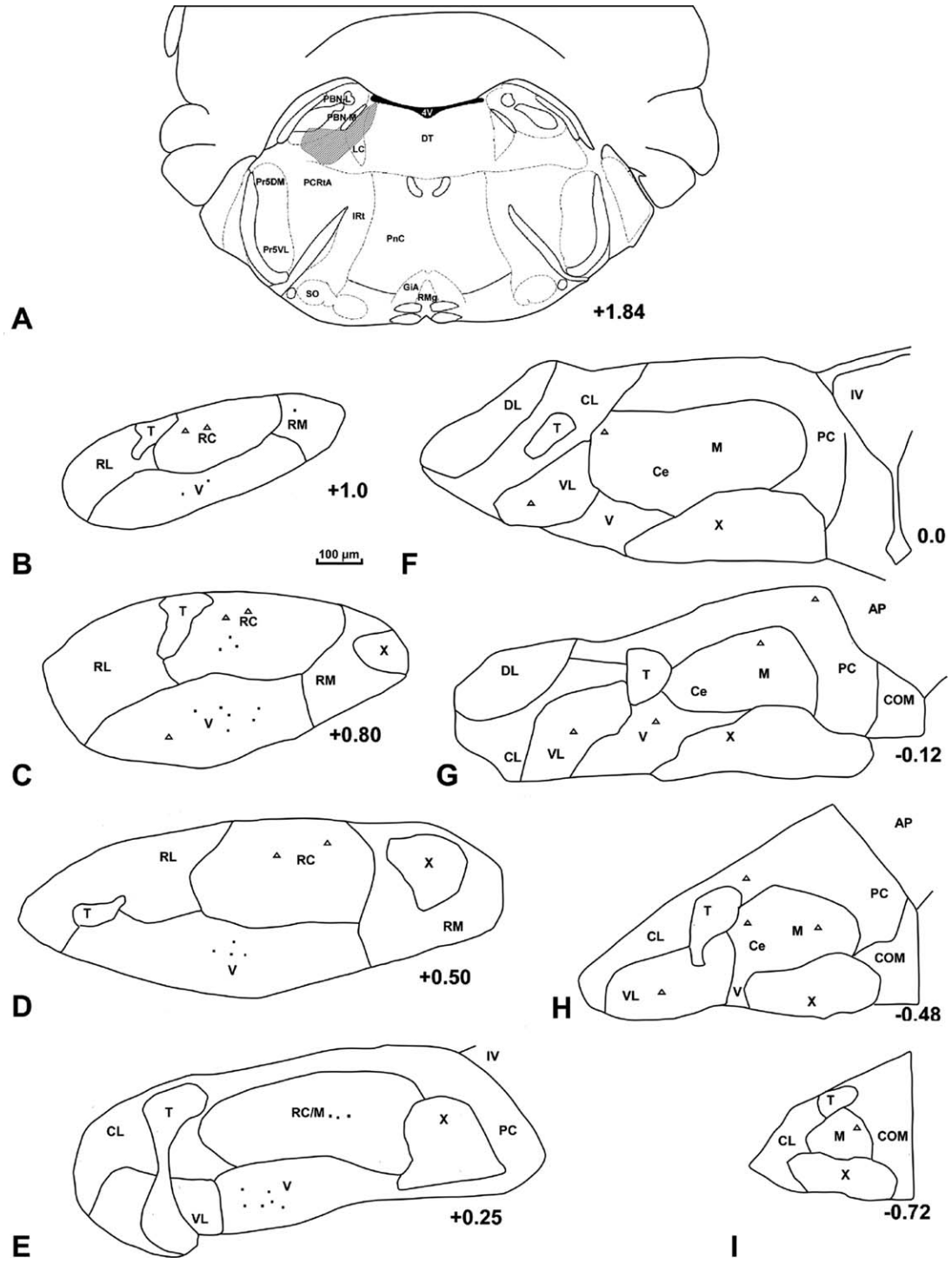

Figure 10. **A–I**: Qualitative plots of retrogradely labeled NST cells (triangles) after a small CTb injection into the lateroventral sector of the medial parabrachial nuclei (uppermost schematic, diagonal lines). The injection also includes the lateral dorsal tegmental nucleus, locus ceruleus, and medial vestibular nucleus. Within the NST, retrogradely labeled somata are mainly in RC and M, with fewer cells in V, and VL. Also, sparse terminal projections (dots) are seen mainly in V, RC, and M within the rostral and anterior intermediate divisions of the NST. For abbreviations see list. Scale bar = 100 µm.

and VL) and PC subnuclei. ANOVA of the proportion of retrogradely labeled cells (n = 323 total cells, labeled and unlabeled) sampled across NST subnuclei does not achieve significance ($H = 7.96$, $df = 9$, $P \geq 0.05$). The small size of this PBN injection is reflected in the sampling of NST subnuclei; only 2.6% (nine of 339 neurons)

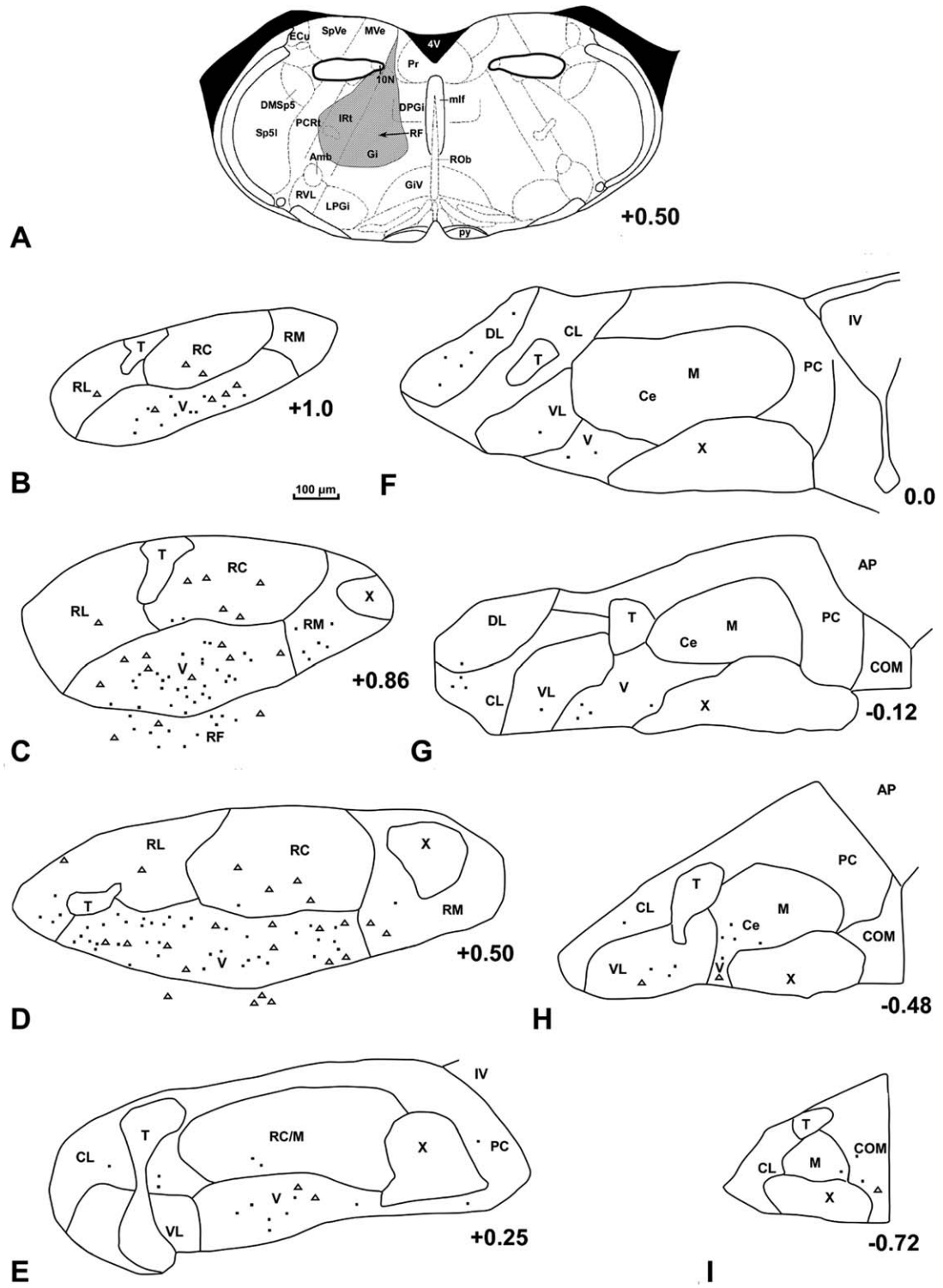

Figure 11. **A–I**: Qualitative plots of retrogradely labeled NST, medullary RF projection cells immediately subjacent to the NST (open triangles), and the RF projection field in the NST (dots) after CTb injection into the medullary RF (uppermost schematic, diagonal lines; schematic adapted from Paxinos and Franklin, 2001). The injection site extends from a medial sector of medial vestibular nucleus (Mve) ventrally to above the nucleus ambiguus (Amb) and does not invade NST. Rostral to the obex, retrogradely labeled somata in the NST subnuclei predominate in V and to a lesser degree in RC. Along the entire rostrocaudal extent of the NST, fewer labeled somata are evident in RL, RM, and VL. RF terminal projection field endings in the NST predominate in V and to a lesser degree in RC, CC, RL, CL, DL, and RM. Retrogradely labeled cells and terminal endings also are evident in the RF subjacent to the V subnucleus of NST. For abbreviations see list. Scale bar = 100 µm.

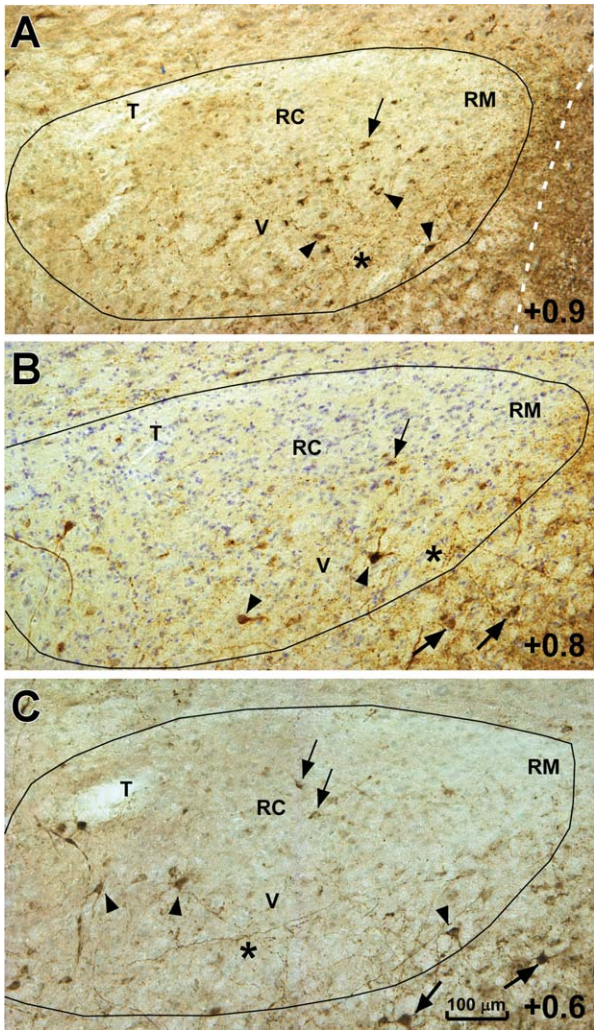

Figure 12. Photomicrographs of retrogradely labeled NST somata and projection field terminations in the rostral division of the NST (outlined) after CTb injection into the medullary RF (same case as in Fig. 11). The dorsal portion of the injection site (dashed line in A) medially borders the rostral medial subnucleus (RM) of NST. In **A–C**, retrogradely labeled NST somata predominate in V (arrowheads) and are larger than the more sparsely labeled cells in RC (thin arrows). Labeled RF projection field endings (asterisks in A–C) are scattered in subnucleus V of the NST. Retrogradely labeled cells also are present in the RF (arrows in B,C) immediately subjacent to the V subnucleus of the NST. Sections B,C are lightly Nissl counterstained. For abbreviations see list. Scale bar = 100 µm.

of the cells are labeled; six of these nine labeled cells are in RC and M. Finally, sparse terminal projections of pontine cells (dots) are seen mainly in V and RC/M within the rostral 0.75 mm (i.e., rostral and anterior intermediate divisions) of NST.

NST-medullary RF connections

Nine cases exhibited injections into the medullary RF subjacent to the rostral division of the NST. Differences in the size and reticular subdivision of the injection are reflected in the number of NST cells labeled but are consistent for the localization of retrograde labeling to identified NST subnuclei. Four additional control cases exhibited injections restricted to the vestibular nuclear complex or rostral pontine RF; few or no NST cells are retrogradely labeled in these latter cases (not shown).

Figure 11 illustrates a representative CTb injection into the RF, 0.50 mm (i.e., at the level of the rostral division of the NST) rostral to the obex. The rostrocaudal extent of the injection is 0.6 mm. The injection site extends dorsally, from a medial sector of medial vestibular nucleus (Mve), to ventrally, above nucleus ambiguus (Amb), and does not invade the NST (Fig. 11, uppermost schematic; see also Fig. 12A). As qualitatively plotted in Figure 11 (triangles), in the rostralmost 0.75 mm (i.e., rostral and anterior intermediate divisions) of the NST, most retrogradely labeled somata are seen in V and to a lesser degree in smaller somata in RC (Figs. 11A–C, 12). Along the entire rostrocaudal extent of the NST, the fewest labeled somata are evident in RL, RM, VL, and COM subnuclei. Kruskal-Wallis ANOVA of the proportion of retrogradely labeled cells ($n = 323$ total cells, labeled and unlabeled) sampled across NST subnuclei is not significant ($H = 12.058$, $df = 9$, $P \geq 0.05$). Sixty-one percent (11 of 18 neurons) of these labeled cells are identified in the V subnucleus.

Mirroring its degree of afferent source from the V subnucleus, medullary RF terminal projection field endings (Figs. 11, dots; 12) predominate in V and to a lesser degree in RC, M, RL, CL, DL, PC, and COM in the NST. Finally, the RF immediately subjacent to the rostral NST shows interconnectivity, limited to a 0.36-mm extent rostrad from the injection site (data not shown).

Intra-NST connections

In six cases, the injected CTb label is entirely confined to the rostral division (three cases), transition zone between intermediate and caudal divisions (two cases) or caudal (one case) division of the NST. In one additional case, the AP was injected (Fig. 13).

Figure 14 illustrates labeling resulting from an injection centered in the rostral division of the NST (see also Fig. 13, case R-1). The injection site coincides with the medial half of the nucleus, 0.5 mm rostral to the obex, and involves a medial portion of RC (Fig. 15A,B), RM, and V subnuclei. Immediately rostral to the injection site, e.g., at +0.8 mm relative to the obex, both retrograde cellular and anterograde axonal terminal labeling are evident in the RL, RC, RM, and V subnuclei (Figs. 13, 15C).

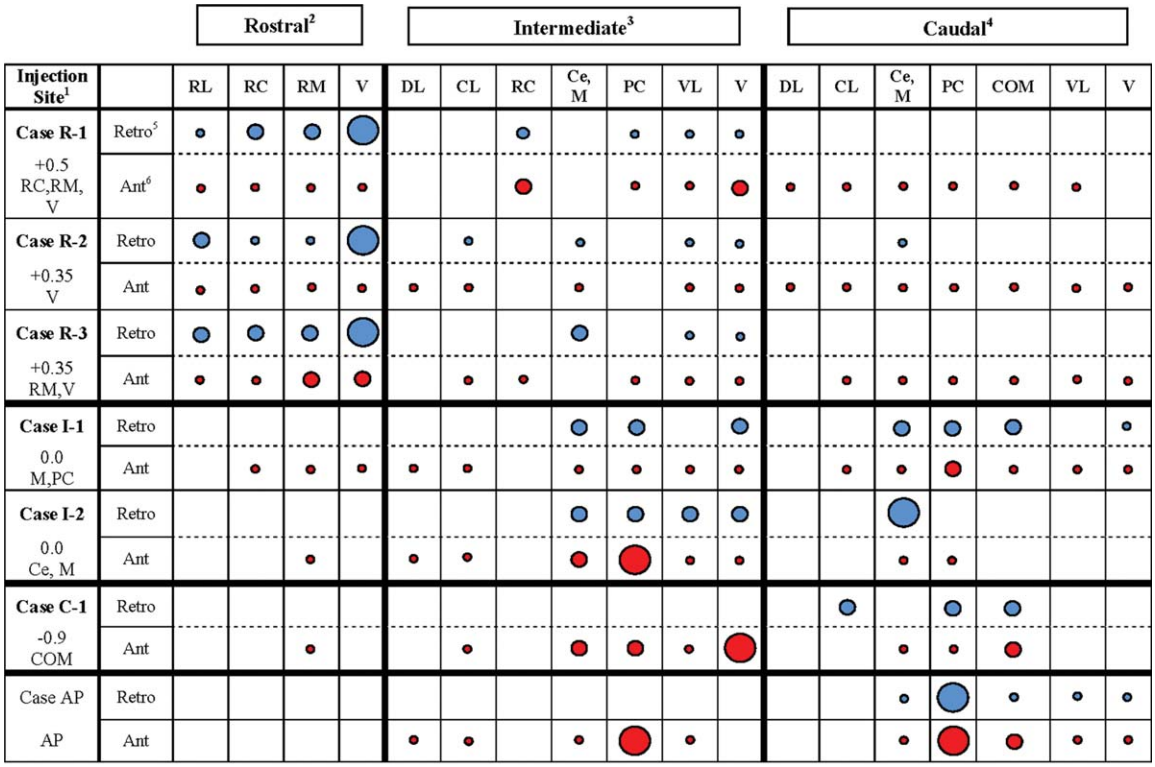

[1]Location and distance from the obex of NST subnuclear, and AP injections.
[2]Subnuclear location of labeling compiled across sections at +1.0, +0.8, and +0.5 relative to the obex.
[3]Subnuclear location of labeling compiled across sections at +0.25 and 0.0.
[4]Subnuclear location of labeling compiled across sections at -0.12, -0.48, and -0.72.
[5]Blue dots = percentages of total retrogradely labeled cells quantified. Small dots = 1-5% of total, medium dots = 6-10% of total, large dots = 11-20% of total. Note: the depicted percentages apply to 2-3 sections/levels per division, each with the degree of labeling shown.
[6]Red dots = percentages of total anterogradely labeled endings. Small dots = 1-2.5% of total, medium dots = 3-5% of total, large dots: 5-10% of total. Note: the depicted percentages apply to 2-3 sections/levels per division, each with the degree of labeling shown.

Thick black lines separate rostral, intermediate, and caudal NST divisions.

Figure 13. Intra-NST connections.

Caudal to the injection site, retrograde cellular labeling is located only nearby caudally, e.g., at 0.25 mm rostral to the obex, that is, at the rostral level of the intermediate division (Fig. 14), primarily in RC, PC, VL, and V (Figs. 13, 15D). Anterograde labeling, however, extends more caudally than retrograde labeling; endings are present as far caudally as −0.72 mm relative to the obex (Fig. 14). Specifically, within the caudal division, anterograde labeling is present in DL, CL, M, PC, COM, and VL subnuclei (Fig. 13). The endings located in M largely exclude and surround Ce (Fig. 15D). Outside the NST, anterograde labeling is present in motor X, motor XII, and the RF (Fig. 14). Rostrally, in the pons, labeled endings are present in the PBN but are sparse and faint (data not shown). Labeling dorsal to the NST, attributable to the track of the pipette containing CTb, is also present in the vestibular nuclei (Fig. 14).

Two other CTb injections into the rostral NST (Fig. 13, cases R-2, R-3) also involve RM and V subnuclei. Compared with the previous case, the injection sites are located slightly more caudally in the rostral division, i.e., both at 0.35 mm rostral to the obex (Fig. 13). Nevertheless, these latter cases demonstrate similar rostral and caudal connections within the NST. In the rostral division, labeled cells and axonal endings are present in subnuclei RL, RC, RM, and V; cells predominate in V in both cases. In the intermediate division, labeled cells are located mainly in subnuclei that continue into (V subnucleus) or lie nearby (VL and M subnuclei) injected subnuclei. Outside the NST, endings

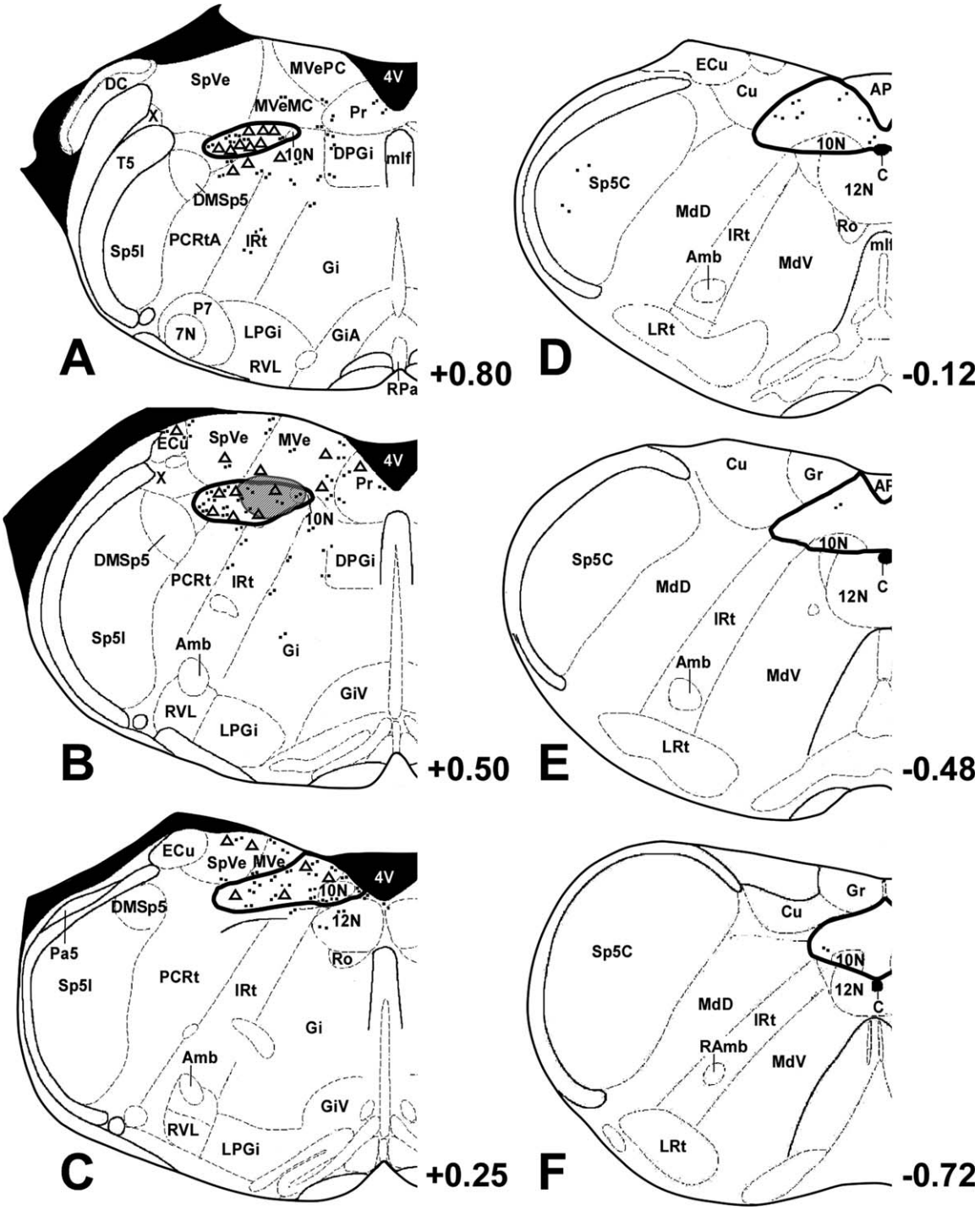

Figure 14. **A–F**: Qualitative plots of retrogradely labeled somata (triangles) and projection field terminals (dots) in the NST and surrounding brainstem regions after CTb injection confined within the rostral division of the NST. The injection site involves RM and the medial half of RC and V (see also Fig. 13, case R-1). Intra-NST connections are evident as labeled cells rostral and immediately caudal to the injection site. Intra-NST terminal projections also extend rostral and caudal to the injection site, essentially overlapping the distribution of retrogradely labeled cells. In addition, some labeled endings extend farther caudally than labeled cells, i.e., throughout the full extent of the caudal division of the NST, becoming sparse at the caudal pole. For abbreviations see list.

extend into motor X and the RF. In case R-2 (Fig. 13), the injection is larger and centered more ventrally; its anterograde labeling also reaching motor V, VII, and XII nuclei and nucleus ambiguus. In general, results of injections in RM, V, and RC in the rostral division indicate that most NST projection cells to these subnuclei

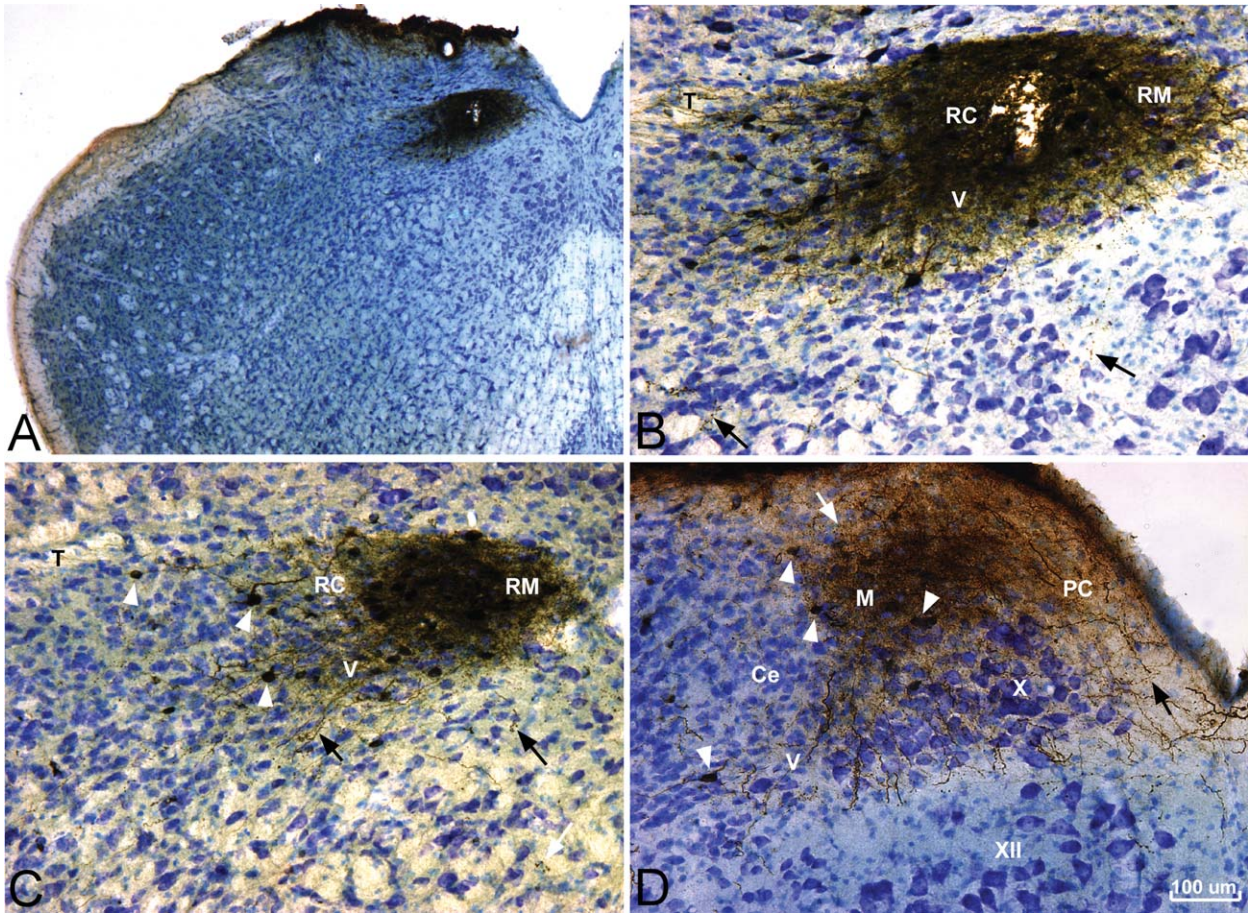

Figure 15. Photomicrographs of the injection site and rostrally and caudally transported labeling in the case plotted in Figure 14. **A,B:** Injection site at low and high magnification essentially fills the medial half of the rostral NST. Labeled endings extend ventrally into the RF (arrows). **C:** Retrogradely labeled cells (arrowheads) and labeled axonal endings (arrows) within the rostral division of the NST, 0.3 mm rostral to the injection site (+0.8 relative to the obex), predominate in RM, RC, and V. **D:** Labeled cells (arrowheads) and endings (arrows) in the rostralmost level of the intermediate division of the NST, 0.25 mm caudal to the injection site (+0.25 relative to the obex), are present in M and V; endings essentially fill M. Transported label mostly spares Ce. Labeled axons and endings are also present in X. For abbreviations see list. Scale bar in D = 100 μm in B-D, 200 μm in A.

are not located caudal to the obex. Moreover, and in contrast to the source of NST projections to RM, V, and RC, these latter subnuclei exhibit terminal projections throughout all subnuclei in all divisions of the NST (Fig. 13).

Figure 16 illustrates labeling resulting from an injection confined to the transitional zone bridging caudal and intermediate divisions of the NST. The injection site is centered medially in the NST at the level of the obex (0.0; Fig. 13, case I-1) and includes PC and the medial half of M. Rostral to the injection site and within the rostral division of the NST, only anterograde labeling is evident. Labeled axonal endings are moderate in RM and sparse in RC and V subnuclei (+0.5; Figs. 13, 16A). Outside the NST at the level of its rostral division, labeled endings are present in the RF; motor VII, motor X, and motor XII nuclei; and nucleus ambiguus (data not shown). At the level of the pons are sparse endings in PBN (data not shown). At the rostral pole (+0.25) of the intermediate division, and immediately caudal (−0.12, caudal division) to the injection site, retrogradely labeled cells and endings predominate in PC, M, and V subnuclei (Figs. 13, 16B,D,E). Farther caudally within the caudal division (−0.48, −0.72) of the NST, axonal endings continue to be evident in PC, M, and V and also COM subnuclei (Fig. 13). Terminal field projections are also evident in the contralateral NST at the level of the AP and caudally (0.0 to −0.72). Outside the NST at levels below the obex, endings are present in the AP (−0.12, −0.48; Fig. 16).

An additional CTb injection (Fig. 13, case I-2), also at the level of the obex, showed a similar pattern of labeled connections involving many of the same NST subnuclei and extra-NST projections as in case I-1

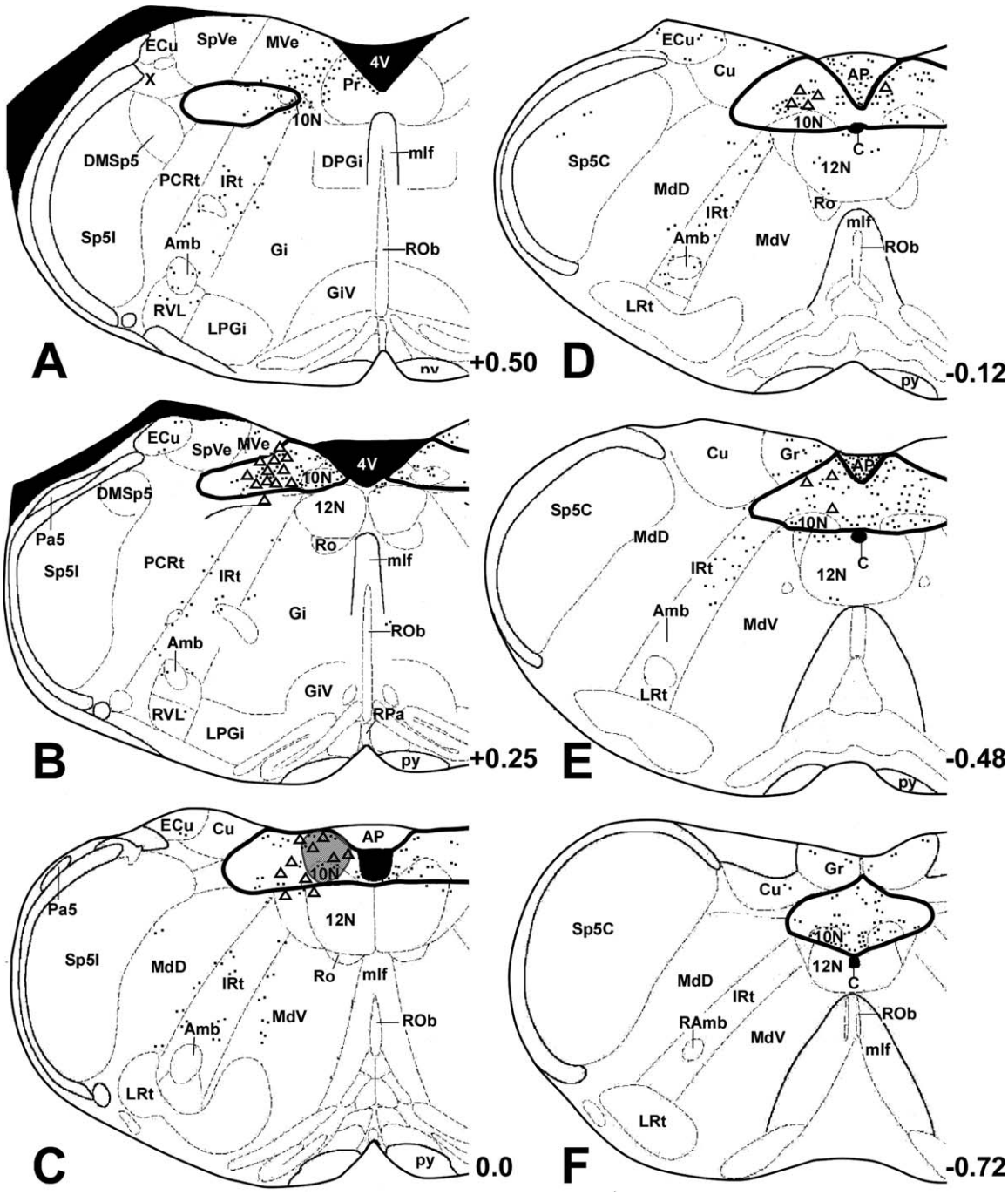

Figure 16. **A–F**: Qualitative plots of retrogradely labeled somata (triangles) and projection field terminals (dots) in the NST and surrounding brainstem regions after CTb injection into the transitional zone between caudal and intermediate divisions of the NST. The injection site involves M and PC at the level of the obex. Retrogradely labeled cells were confined to the caudal division and were limited in extent to 0.25 mm rostral, and 0.48 mm caudal to the injection site, respectively. Intra-NST labeled axonal endings were more extensive, reaching both the rostral pole (not shown), where they predominated medially; throughout the caudal division, where they predominated in M, PC, and V; and at the caudal pole, in COM. Endings of NST projections within the medulla were seen in the area postrema, the RF, motor X and XII nuclei, and nucleus ambiguus. For abbreviations see list.

(Fig. 13). The injection site was smaller and slightly more dorsal than that in the previous case. Thus, by contrast, extra NST projections did not include motor VII or motor XII nuclei or nucleus ambiguus. As in case I-1, the rostral division of the NST contains only anterogradely labeled axonal endings, here present only in RM. Within the intermediate division immediately rostral to the injection site, and the caudal division,

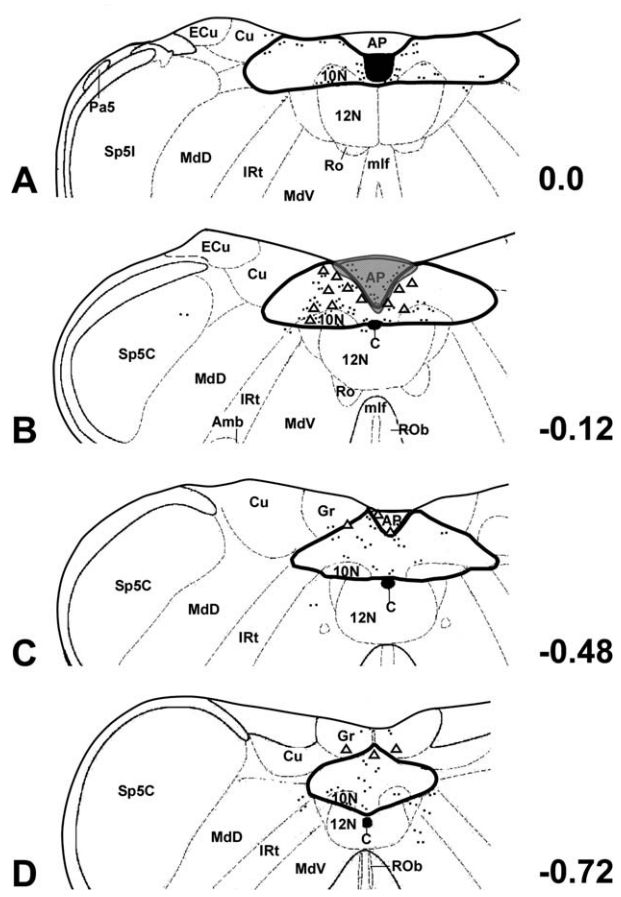

Figure 17. **A–D**: Qualitative plots of retrogradely labeled somata (triangles) and projection field terminals (dots) in the NST after CTb injection confined to the area postrema caudal to the obex (shaded area in the dorsal median plane at −0.12). Retrogradely labeled cells were mostly confined to the NST at the level of the injection site, primarily in M and PC. Labeled axonal endings were confined the caudal division of the NST, where they were distributed throughout its extent, primarily in PC and also in M, VL, V, and COM. For abbreviations see list.

retrogradely labeled cells and endings are present in PC, M, VL, and V subnuclei. Projections also are seen in DL, CL, and COM (Fig. 13, case I-2).

A CTb injection within the caudal division of the NST is located near the caudal pole of the NST, centered in COM at −0.90 relative to the obex (Fig. 13, case C-1). Projections, only, are evident rostrally in the intermediate and rostral (only in RM subnucleus) divisions. In contrast, both retrogradely labeled cells and endings are restricted to the caudal division of the NST. Labeled cells are identified in CL, PC, and COM subnuclei, at −0.72 and −0.48 relative to the obex. Axonal endings are present in M, PC, and COM subnuclei immediately rostral to the injection site.

An injection of the rostral AP (−0.12; Fig. 13, case AP) results in both retrogradely labeled cells and labeled axonal endings restricted to the caudal division of the NST, in PC, M, VL, and V subnuclei (Fig. 13). Labeled cells are seen from −0.12 to −0.72 caudal to the obex (0.0; Fig. 17). Endings extend from the caudal pole of the NST to the obex (0.0) but no farther rostrally; DL and CL subnuclei also exhibit endings at the obex level. The pons was not evaluated in this case.

DISCUSSION

Anterior tongue afferents of NST subnuclei

Comparing the gustatory NST across studies that vary in labeling technique or method of tongue stimulation sometimes is hampered by using only regional (e.g., rostral, lateral, anteromedial) descriptions. Table 2 compares the terminology of NST subnuclei in the present study with that in previous selected studies in rodents.

With the cytoarchitectonic subnuclear parcellation of the entire NST in mouse as a referent, the CT was selected to demonstrate the full extent of the anterior tongue fungiform/anterior posterolateral foliate taste bud projection field in NST that includes a minor somatosensory component (rat: Contreras et al., 1982; hamster: Whitehead and Frank, 1983). The present CTb injection data indicate that the chorda tympani nerve (CT) terminates most densely in the dorsal halves of RC and M; is relatively less dense in RL; and is least dense in V, VL, and CL subnuclei of the NST. Based on recent studies in the rat showing extensive overlap of the subnuclear targets in NST of CT and greater superficial petrosal (GSP) branches of the facial and glossopharyngeal (IX) nerves (May and Hill, 2006; Corson et al., 2012), it is expected that further studies in the mouse will show that terminal field projections of GSP and IX nerves similarly will show extensive overlap in RC and RL and less so in VL subnuclei of the rostral and intermediate divisions of NST; CT projects farther caudally into VL and M subnuclei in the rostral portion of the caudal division of NST (this report; cf. rat: Corson et al., 2012).

Table 3 summarizes anterior tongue projections to the NST in the present study with previous reports in rodents in which detailed photomicrographs and terminal field projection plots clearly depict the distribution of label or evoked response in the NST. Included in Table 3 are targets in the NST using whole-mouth tastant stimulation. In mouse, it can be seen that the present Ctb labeling data provide the fullest rostrocaudal extent of the CT terminal projection field in NST and may relate to the nature of the tracer used. Ctb is reportedly more efficient at labeling axonal projections by anterograde transport than other labeling methods

TABLE 2.

Comparative Cytoarchitectonic Parcellation in Selected Regions of NST in Rodents

Mouse	Hamster	Rat		
Present study; Zaidi et al., 2008[1]	Whitehead, 1988[1–3]	Torvik, 1956[1,2]	Kalia and Sullivan, 1982; Ross et al., 1985; Cunningham and Sawchenko, 1989; Zhang and Ashwell, 2001a[1,4]	Herbert et al., 1990[1]
Central (RC, Ce[5,6])	Central (RC and CC)	Medial[7]	Intermediate,[8] central[9]	Central[4,5,10]
Commissural		Medial	Commissural	Commissural
Dorsolateral(DL)	Dorsolateral	Lateral[7]	Dorsolateral	—[11]
Lateral (RL and CL)	Lateral (RL and CL)	Lateral	Interstitial	
Medial	Caudal central	Medial	Medial	Medial
Parvicellular[5]	Medial	Medial	commissural	Parvicellular[5]
(PC)	Medial	Medial	Medial,[8] central[10]	
Rostral medial[7]				
Ventral	Ventral		Ventral	—[11]
Ventrolateral	Ventrolateral	Lateral	Ventrolateral	Ventrolateral

[1]Nissl.
[2]Silver.
[3]Golgi.
[4]See Discussion.
[5]Distinguished by moderate to dark staining for NADPH-diaphorase.
[6]Distinguished by intense $P2X_2$ immunoreactivity.
[7]Medial and lateral divisions of NST.
[8]According to Kalia and Sullivan (1982).
[9]According to Zhang and Ashwell (2001).
[10]Identified in Nissl material and its specific projection to nucleus ambiguus as distinct from within the medial subnucleus of Kalia and Sullivan (1982).
[11]According to Herbert et al. (1990), dorsolateral and ventral subnuclei are not distinguishable from ventrolateral nucleus proper in Nissl (thionin) stain.

(Vercelli et al., 2000), although this may apply more to primary afferent axons than to axons of labeled CNS neurons. Also, methodological and strain differences notwithstanding, it may be that most murine studies have not included in their analyses the anterior tongue projections to the M, VL, and V subnuclei in intermediate and caudal divisions of NST. In rat, it appears that the fuller extent of the CT terminal projection field in NST usually is obtained with transported markers applied to the CT, as in the present study, or injected into the geniculate ganglion vs. anterior tongue injection or whole mouth, taste stimulation.

Notwithstanding the absence of formally defined NST subnuclei in some previous studies, it may be concluded from Table 3 that the CT in rodents projects to similar locations in the NST, mainly to its rostral division as described here. Studies are consistent in that the caudal extent of the CT terminal projection field reaches to the obex, whereas the projections at the rostral pole of the NST abut and/or extend into the dorsomedial cap of spinal trigeminal nucleus oralis (also in cat; Nomura and Mizuno, 1981, 1983). Supporting the results above, our analysis of coordinates reported for single-unit responses in the rostral division of the NST to tongue taste stimulation in C57BL/6J mice (McCaughey, 2007) suggests that taste-responsive cells were located in the rostral one-fourth of the RC subnucleus. Similarly, in rat, whole-tongue, taste-solution stimulation of fungiform, foliate, and circumvallate taste buds evoked responses in the lateral half of the rostral NST at the 'rostral poles of the NTS' (Monroe and Di Lorenzo, 1995, p. 252).

NST connections with PBN

The present data in C57BL/6J mouse indicate that relatively large iontophoretic CTb injections that included the recently described gustatory (Tokita et al., 2011) and expected tongue tactile/viscerosensory regions of lateral and medial parabrachial nuclei in the C57BL/6J mouse retrogradely labeled cells in RC and M, V, RL, VL, PC, CL, and RM subnuclei of NST, with RC and M providing the largest source of PBN afferents from NST (cf. Sprague-Dawley rat: Karimnamazi et al., 2002). Similarly, a small injection into the lateroventral sector of the medial parabrachial nuclei also showed that mainly RC and M cells, and fewer cells in V, VL, and PC subnuclei, were retrogradely labeled. This smaller injection might have missed taste-responsive neurons located in more dorsal and medial regions of the medial parabrachial nuclei and may account for the relative paucity of retrogradely labeled cells in the NST

TABLE 3.

Anterior Tongue Projections to, Immunoreactivity, and Transgene Expression in NST in Rodents

Rodent strain	Technique	Extent[1] and/or location[2] in NST	Citation
Mouse			
C57BL/6NCr1BR	HRP-injected anterior tongue	~0.48 mm[1,*]; ~0.15 mm[1,**]	Kachele and Lasiter, 1990
C57BL/6J	$P2X_2$ immunolabeling	RC[2]	Bartel et al., 2007
GAD1-EGFP	Fos-like immunoreactivity to whole mouth, taste stimulation	Medial third, rostral NST[2]	Travers et al., 2007
Wild-type	Fos-like immunoreactivity to linoleic acid on the tongue	Central and ventrolateral, rostral NST[2]	Gaillard et al., 2008
tr1r3-WGA	WGA transgene expression	RC (dorsal half)[2]	Ohmoto et al., 2008
C57/1bl6	Pseudorabies virus 823-injected fungiform papillae	RC > RL, CL > V > M, RM[2,3]	Zaidi et al., 2008
P2X double knockout and wild type	Fos-like immunoreactivity to whole mouth, taste stimulation	1.2 mm[1,2]; rostral and caudal divisions of NST	Stratford and Finger, 2011
C57BL/6J	CTb-labeled CT	1.1 mm[1] RC, M > RL > V, VL, CL[2]	Present study
Hamster			
Syrian	HRP applied to CT	2.4 mm[1]; dorsal half, rostral NST > lateral half, caudal NST[2]	Whitehead and Frank, 1983
Syrian	Anterior tongue, taste stimulation and NST electrophysiology	RC, RL[2]	McPheeters et al., 1990
Rat			
Albino	Intermediate facial nerve avulsion; Nauta silver method	Medial and lateral divisions, rostral NST[2]	Torvik, 1956
Sprague-Dawley	[^{3}H]proline- or leucine-injected geniculate ganglion	2.5 mm[1,*]; lateral division of mainly rostral NST[2,4,5]	Contreras et al., 1982
Sprague-Dawley	HRP applied to CT	2.8 mm[1,*]; lateral > medial division of mainly rostral NST[2,4,6]	Hamilton and Norgren, 1984
Sprague-Dawley	Whole mouth, taste stimulation and NST electrophysiology	0.4 mm[1]; rostrocentral NST[2]	Ogawa et al., 1984
Sprague-Dawley	Fos-like immunoreactivity to whole mouth, taste stimulation	RC, rostral NST	Harrer and Travers, 1996
Wistar	DiI applied to facial nerve, or inserted into anterior tongue	VL, V (obex/AP levels)[2,7]	Zhang and Ashwell, 2001
Sprague-Dawley	CTb-injected anterior tongue	1.4 mm[1,*]; dorsal two-thirds, rostrolateral NST	Hayakawa et al., 2003
Sprague-Dawley	Tetramethylrhodamine dextran amine applied to CT	~0.35 mm[1,*]; rostral NST[2]	May and Hill, 2006
Sprague-Dawley	Biotinylated dextran amine applied to CT	3.0 mm[1,*]; RC, RL, VL[2]	Corson et al., 2012

[1]Rostrocaudal extent in NST notwithstanding absence or difference in definition of the obex compared with the present study.
[2]Localization in NST subnuclei or regions of NST. Relative degree of projections in NST subnuclei listed as dense to sparse.
[3]NST subnuclear nomenclature of Ganchrow et al. (2007) and the present study.
[4]NST divisions of Torvik (1956).
[5]Terminal projection field concentrated dorsoventrally (coronal sections).
[6]Dorsoventral terminal projection field in lateral NST > dorsal concentration in medial NST (coronal sections).
[7]NST subnuclear nomenclature of Kalia and Sullivan (1982; see Table 1). Rostral NST was not examined.
*As determined from horizontal schematics or images.
**Dorsoventral plane as calculated from horizontal sections.

subnuclei (cf. our Fig. 10 with Tokita et al., 2012, Fig. 9, p. 1552; see also Travers et al., 2007). In general, the present results are consistent with fluorescent marker and autoradiographic data in the same mouse (Tokita et al., 2009), Sprague-Dawley and Wistar rat (Halsell et al., 1996; Harrer and Travers, 1996; Williams et al., 1996; Gill et al., 1999; Travers and Hu, 2000; Hermes et al., 2006), and Syrian hamster (Whitehead, 1990) strains showing that injections either restricted to the midcentral PBN and including the superior cerebellar peduncle of the "waist" area (Halsell and Travers, 1997) or including structures surrounding PBN proper consistently label RC, RM, RL, and V subnuclei of NST. M, PC, and COM subnuclei in the caudal division of NST are more heavily labeled after injections centered in lateral PBN (Whitehead, 1990). Notably, in these studies in rodents, although the proportions of labeled cells in these subnuclei might differ slightly, RC cells

provide at least one-half of the NST projection cell population to the PBN (cf. in hamster: Cho and Li, 2008). Cumulatively, these reports complement earlier anterograde silver degeneration (Norgren and Leonard, 1973) and autoradiographic (Norgren, 1978; Hamilton and Norgren, 1984) studies showing that the taste-responsive region in rostralmost NST, at the level of the dorsal cochlear nucleus, projects to medial and lateral divisions of PBN.

Herbert et al. (1990) reported that in Sprague-Dawley rats after large WGA-HRP pressure injections that include most of the PBN complex, at levels rostral to the obex, many retrogradely labeled cells in NST are located in the "intermediate" subnucleus (nomenclature of Kalia and Sullivan, 1982). The intermediate subnucleus in rat topographically lies ventromedial to the solitary tract and dorsolateral to central subnucleus but cannot be identified in mouse in the present report. Interestingly, analysis of their schematic rostralmost NST sections at ~1.7–2.9 mm rostral to the obex (cf. Paxinos and Watson, 2007) shows that, ipsilaterally, most of NST proper is retrogradely labeled (Herbert et al., 1990, Fig. 2I,K, p. 545). Consistent with their retrograde labeling data, injections covering the lateral two-thirds of rostral NST result in extensive anterograde axonal and terminal labeling in lateral and medial regions of PBN (Herbert et al., 1990, Figs. 19, 20, pp. 561–562, and Fig. 31, p. 575). Unfortunately, cytoarchitectonic Nissl delineation of NST subnuclei at more rostral levels is not shown, and a rostrolateral (RL) subnucleus is not described in their report. Nevertheless, the present authors suggest that the Herbert and coworkers' and the present data in rostral NST are congruent in that "RC" and "RL" project to PBN (cf. Herbert et al., 1990, Fig. 2I,K, p. 545 and our Figs. 8, 10; see also Paxinos and Franklin, 2001, Figs. 85, 88; and Jones, 2005: Allen online brain map atlas, *Mus musculus*, coronal data set Fig. 17c,e).

Similarly, in caudal NST, retrograde and anterograde evidence in the Herbert et al. (1990) study indicate that ventrolateral (VL) subnucleus at the AP level projects to the lateral and medial parabrachial nuclei continuous with as well as within Kölliker-Fuse nucleus (Herbert et al., 1990, Fig. 2, p. 545, and Fig. 14, p. 556). These results are consistent with this report in mouse showing that caudal VL at the AP/obex level receives CT afferents and projects to PBN (cf. Figs. 6–9, this report). VL also may independently project to Kölliker-Fuse nucleus (cf. Herbert et al., 1990; our Fig. 9).

With respect to pontine terminal field projections to V subnucleus, the likely source of the endings is either the PBN proper or the pontine RF. Evidence favoring an RF source is that the NST endings are dense only after PBN injections that also include the adjacent RF. Moreover, the anterograde labeling in the pons nearby the injection sites extends into the motor trigeminal nucleus (data not shown) and is coextensive with labeling of cells and endings in the RF extending throughout the pons and rostral medulla. In addition, although we cannot entirely rule out the interpretation that some minor, linearly appearing labeling in the NST after pontine injection may be axon collaterals or dendrites of *retrogradely* labeled somata of other NST subnuclei, this would represent a minor portion of the terminal field appearance of CTb labeling in the rostral subdivision of NST. Golgi-Cox/Nissl preparations in hamster NST show that the dendritic spread in the coronal plane of RC cells predominantly remains confined within RC, with rare invasion into the dorsalmost region of ventrally adjacent V subnucleus (Whitehead, 1988; see also in hamster: Davis, 1988). The average dendritic length of biocytin-filled rostral NST neurons in rat is ~600 μm, but only ~20% (12 of 58 cells) of neurons exhibit dendritic spread ventrally in the coronal plane (King and Bradley, 1994). Therefore, V and, to a lesser extent, RM subnuclei in NST are targeted for feedback from the PBN or pontine RF.

NST connections with the RF

Injections of the RF ventral to the *rostral* NST retrogradely labeled cells in RC, M, and V (Figs. 10, 11). This establishes for the mouse a local intramedullary circuit whereby certain NST subnuclei engage premotor effectors that, in turn, e.g., activate muscles involved in feeding behavior or modulate autonomic outflow (see also for mouse: Zaidi et al., 2008; hamster: Whitehead et al., 2000; rat: Norgren, 1978; Becker, 1992; Kinzeler and Travers, 2008). This local circuitry includes premotor cells in RC (and the RF) that are NADPH-diaphorase positive (Travers and Travers, 2007), consistent with the present NADPH-diaphorase staining of RC in mouse. With respect to RC, tranganglionic viral labeling initiated in fungiform taste buds indicates that these RC cells are distinct from those in RC that project to the PBN in that the two projection neuron types receive inputs from different geniculate ganglion cell types (Zaidi et al., 2008; see also Yamamoto et al., 2011). The present data suggest that RC-RF projection cells are scattered within the ventral half, whereas geniculate ganglion-RC projection cells are densely packed within the dorsal half of RC (cf. Figs. 6, 11). Thus, the RC neuronal population might possibly be distinguished by a segregation of ascending pontine- and local intramedulla-projecting neurons. The present report indicates that, in contrast to RC, the V subnucleus receives a very minor CT input, located only at the

obex level. Though similar to RC with respect to projections to the subjacent RF in the rostral NST, subnucleus V appears to be more strongly reciprocally linked to the RF by receiving predominant RF terminal field projections (cf. Figs. 6, 11). In other rodents, subnucleus V also receives taste RC and RL afferents (cf. in mouse: Zaidi et al., 2008; hamster: Whitehead et al., 2000; rat: Norgren, 1978; Becker, 1992). Thus, to different degrees, the RC and V subnuclei link the gustatory anterior tongue-rostral NST to the medullary RF and brainstem circuitry mediating reflexive oromotor responses (Beckman and Whitehead, 1991; Halsell et al., 1996; Nasse et al., 2008; Zaidi et al., 2008).

With regard to the *caudal* NST, anterograde transport in the present study established that the caudal division of the NST in mouse also projects to the RF at that level. Caudal NST projections to the subjacent RF have also been demonstrated in cat (Morest, 1967), a connection mediating general visceromotor outflow.

The central subnucleus (Ce) and $P2X_2$ IR in caudal NST

Ce in the mouse, as in the "central" subnucleus (Ce) of rat, is characterized by a distinctive, relatively more intense NADPH-diaphorase staining of its neuropil compared with surrounding NST subnuclei (Herbert et al., 1990, Fig. 1A,B, p. 544; Broussard et al., 1995, Fig. 1C,F, p. 2075; Sang and Goyal, 2001, Figs. 2F, 3B, pp. G194–G195). Other histochemical markers for Ce in rodents include 1) calbindin IR (mouse: Okada et al., 2008; rat: Zhang and Ashwell, 2001; 2) glutamate decarboxylase 67 and $GABA_A$ expression (mouse: Okada et al., 2008; rat: Broussard et al., 1996) and $GABA_A$-IR (rat: Terai et al., 1997); and 3) calretinin and substance P immunonegativity relative to surrounding NST subnuclei (rat: Zhang and Ashwell, 2001). Ce in rat has specific connections with ambiguus/periambiguus nuclei and does not project to the PBN (Ross et al., 1985; Cunningham and Sawchenko, 1989; Herbert et al., 1990, Figs. 1A, 2G,H, 4, 5, pp. 544–548).

$P2X_2$, an ionotropic receptor for ATP, was used in the present study to characterize further the subnuclei of mouse caudal NST. $P2X_2$-IR is localized to many fibers of the solitary tract of probable vagal nerve origin at intermediate/caudal levels and is particularly intense in solitary tract preterminal axons and endings within the Ce subnucleus. Consistent with this, CTb or WGA applied to the subdiaphragmatic esophagus of rat labels vagal nerve afferents that end in and form axodendritic synapses within Ce (Altschuler et al., 1989; Hayakawa et al., 2003). Other studies have shown that $P2X_2$-IR is evident in vagal ganglion cells and distal processes innervating esophageal and intestinal mucosa involved in gastrointestinal function such as mechanoreceptive-elicited peristalsis (mouse: Kestler et al., 2009; rat: Wang and Neuhuber, 2003). Centrally, $P2X_2$-IR is seen in the rat solitary tract at caudal NST levels, where vagal axons predominate, and, in an unidentified, round field ventromedial to the solitary tract that appears to coincide with the region of Ce as shown here (Atkinson et al., 2000; see also for rat: Kanjhan et al., 1999; Yao et al., 2001). Vagal nerve transection significantly reduces the intensity of $P2X_2$ IR in this field in NST compared with the intact contralateral side (Atkinson et al., 2000). Based on the cytoarchitectonic parcellation and $P2X_2$ IR presented here for the caudal (viscerosensory) division of NST and results in rat (Kalia and Sullivan, 1982; Higgins et al., 1984), it is expected that vagal sensory afferents in mouse will project to Ce, M, VL, V, COM, and possibly CL subnuclei (cf. in rat: Contreras et al., 1982; Hamilton and Norgren, 1984).

Thus, as in rat, the vagus nerve and Ce of mouse may form part of the afferent limb of an ATP neurotransmitter-$P2X_2$ receptor-based circuit whose efferent limb is completed by innervation of the esophageal musculature by way of ambiguus nucleus. Whether Ce of mouse specifically exhibits connections with the esophageal motoneuronal pool in ambiguus nucleus is not known; anterograde endings are evident in ambiguus nucleus after an RF injection that includes Ce subnucleus (data not shown here; see in rat: Ross et al., 1985; Cunningham and Sawchenko, 1989; Herbert et al., 1990). The present results are consistent with the aforementioned neural circuit in that 1) CT projections target only the dorsal regions of M and RC that lie dorsal to Ce (cf. Figs. 1, 6, 7) and 2) the region occupied by Ce lying ventromedial to the solitary tract does not project to PBN (cf. Figs. 1, 8, 9D).

Intranuclear connections within the NST

As well as receiving CT afferents and directly projecting to the PBN and RF, the subnuclei of the rostral division of the NST may process intranuclear information within NST proper. With respect to possible intrarostral division connections, this report on C57BL/6J mouse shows that the CT projection field is restricted to the dorsal half of RC, whereas RC projection cells to PBN are more uniformly distributed throughout this subnucleus. In addition, the ventral sector of RC receives a projection from the PBN proper. Arguably, then, some projection cells to PBN in the ventral halves of RC may be at least "third-order" neurons within their regions in the sense that they do not directly receive CT afferents. Alternatively, although not exclusively, the ventral

sector of RC may include, in part, afferents of the greater superficial petrosal branch (GSP) of the facial nerve, because the GSP terminal projection field in NST overlaps and extends more ventrally than that of the CT (rat: May and Hill, 2006; cf. Corson et al., 2012). In addition, in the rostrocentral subdivision (hamster and rat nomenclature) of NST in the GIN transgenic mouse, CT terminal field axons and endings are distributed immediately dorsal to GABAergic cells in the ventral subdivision (Wang and Bradley, 2010). This suggests that, at least in rostral NST, GABA-mediated inhibitory interneurons lie in close proximity to second-order gustatory cells but does not rule out the possibility of convergent inhibitory afferentation of NST cells by different peripheral taste nerves (Suwabe and Bradley, 2009; Corson et al., 2012).

To what degree do anterior and posterior tongue regions interact in NST? In general, the present results show that subnuclei covering the medial half of rostral and intermediate divisions of the NST project within all three divisions of the NST. Specifically, medial RC, RM, and V subnuclei in the rostral division and medial M and PC subnuclei at the obex level exhibit axonal endings extending as far caudally as −0.72 within the caudal division of NST. Inasmuch as RC and M subnuclei receive peripheral taste afferents, taste-activated neurons may possibly engage general viscerosensory cells either by direct or by interneuronal connections. Fluorescent marker, CTb, and HRP injection studies in rat (Halsell et al., 1996; Karimnamazi et al., 2002) and hamster (Whitehead et al., 2000; cf. also in hamster: Travers, 1988; Beckman and Whitehead, 1991) show connections between RC and gastric distention-responsive regions in (what the present authors interpret to be) M and PC subnuclei at the obex/AP level. Conversely, caudal division afferents of the rostral division appear to be minimal and are reflected by sparse obex, COM subnucleus, or rostral AP efferents to the rostral division of the NST (Fig. 13; Morest, 1960; Herbert et al., 1990) Notwithstanding the limited number of CTb injections within the caudal division proper reported here, it is suggested that the rostral division commands a top-down influence on viscerosensory NST via direct or interneuronal connections (Beckman and Whitehead, 1991).

In conclusion, intranuclear connections within the NST revealed with the present Ctb labeling were demonstrated with anterograde labeling that was sometimes more extensive in distribution than could be verified by expected retrograde labeling of cells after appropriate placement of injection sites. This could be explained by the observation that, in the present application, Ctb appears more efficient at anterograde labeling of axons than retrograde labeling of cell bodies and possibly related to differential distribution of membrane sites of entry of the marker (Vecelli et al., 2000). Future study of the details of intra-NST connections with CTb utilizing additional survival times or with other markers is warranted. The present report is intended to facilitate such studies.

ACKNOWLEDGMENTS

We thank Tom Finger for reading an earlier version of the manuscript and sharing unpublished immunocytochemical data, the distribution of which complements the present subnuclear parcellation of NST in the C57BL/6J mouse. We also thank Harvey Karten, Alicia Fritchle, and Dov Ganchrow for invaluable technical consultations. Furthermore, we thank the reviewers and editors for their cogent and thoughtful comments.

CONFLICT OF INTEREST STATEMENT

The authors declare no conflicts of interest.

ROLE OF AUTHORS

DG, JRG, and MCW conceived and designed the study, and prepared the initial drafts of the manuscript. VC, DK, and DG carried out the Ctb, and NADPH experiments, prepared the Nissl atlas, and analyzed data. DLB performed $P2X_2$ experiments and contributed to revision of the draft manuscript. All authors have agreed to the final content and submission of the manuscript.

LITERATURE CITED

Abercrombie M. 1946. Estimation of nuclear population from microtome sections. Anat Rec 94:239–247.

Altschuler SM, Bao X, Bieger D, Hopkins DA, Miselis RR. 1989. Viscerotopic representation of the upper alimentary tract in the rat: sensory ganglia and nuclei of the solitary and spinal trigeminal tracts. J Comp Neurol 283: 248–268.

Angelucci A, Clasca F, Sur M. 1996. Anterograde axonal tracing with the subunit B of cholera toxin: a highly sensitive immunohistochemical protocol for revealing fine axonal morphology in adult and neonatal brains. J Neurosci Methods 65:101–112.

Atkinson L, Batten TF, Deuchars J. 2000. $P2X_2$ receptor immunoreactivity in the dorsal vagal complex and area postrema of the rat. Neuroscience 99:683–696.

Bartel DL. 2012. Glial responses after chorda tympani injury. J Comp Neurol 520:2712–2729.

Bartel DL, Whitehead MC, Finger TE. 2007. Immunohistological map of the nucleus of the solitary tract (NTS) in mice. Chem Senses 32:A110.

Becker DC. 1992. Efferent projections of electrophysiologically identified regions of the rostral nucleus of the solitary tract in the rat. Masters thesis, Ohio State Univresity, Columbus, OH.

Beckman ME, Whitehead MC. 1991. Intramedullary connections of the rostral nucleus of the solitary tract in the hamster. Brain Res 557:265–279.

Bo X, Alavi A, Xiang Z, Oglesy I, Ford A, Burnstock G. 1999. Localization of ATP-gated $P2X_2$ and $P2X_3$ receptor immunoreactive nerves in rat taste buds. Neuroreport 10: 1107–1111.

Broussard DL, Bao X, Li X, Altschuler SM. 1995. Co-localization of NOS and NMDA receptor in esophageal premotor neurons of the rat. Neuroreport 6:2073–2076.

Broussard DL, Li X, Altschuler SM. 1996. Localization of $GABA_A1$ mRNA subunit in the brainstem nuclei controlling esophageal peristalsis. Brain Res Mol Brain Res 40: 143–147.

Chandrashekar J, Hoon MA, Ryba NJP, Zuker CS. 2006. The receptors and cells for mammalian taste. Nature 444: 288–294.

Chen X, Gabitto M, Peng Y, Ryba NJ, Zuker CS. 2011. A gustotopic map of taste qualities in the mammalian brain. Science 333:1262–1266.

Cho YK, Li C-S. 2008. Gustatory neural circuitry in the hamster brain stem. J Neurophysiol 100:1007–1019.

Contreras RJ, Gomez MM, Norgren R. 1980. Central origins of cranial nerve parasympathetic neurons in the rat. J Comp Neurol 190:373–394.

Contreras RJ, Beckstead RM, Norgren R. 1982. The central projections of the trigeminal, facial, glossopharyngeal and vagus nerves: an autoradiographic study in the rat. J Autonom Nerv Syst 6:303–322.

Corson JA, Aldridge A, Wilmoth K, Erisir A. 2012. A survey of oral cavity afferents to the rat nucleus tractus solitarii. J Comp Neurol 520:495–527.

Cunningham ET Jr, Sawchenko PE. 1989. A circumscribed projection from the nucleus of the solitary tract to the nucleus ambiguus in the rat: anatomical evidence for somatostatin-28-immunoreactive interneurons subserving reflex control of esophageal motility. J Neurosci 9:1668–1682.

Davis BJ. 1988. Computer-generated rotation analyses reveal a key three-dimensional feature of the nucleus of the solitary tract. Brain Res Bull 20:545–548.

Damak S, Mosinger B, Margolskee R F. 2008. Transsynaptic transport of wheat germ agglutinin expressed in a subset of type II taste cells of transgenic mice. BMC Neurosci 9:96.

Finger TE, Danilova V, Barrows J, Bartel DL, Vigers AJ, Stone L, Hellekant G, Kinnamon S. 2005. ATP signaling is crucial for communication from taste buds to gustatory nerves. Science 310:1495–1499.

Ganchrow D, Ganchrow J, Warner N, Whitehead M. 2007. The mouse NST: a cytoarchitectonic atlas. Chem Senses 32: A110.

Gill CF, Madden JM, Roberts BP, Evans LD, King MS. 1999. A subpopulation of neurons in the rat rostral nucleus of the solitary tract that project to the parabrachial nucleus express glutamate-like immunoreactivity. Brain Res 821:251–262.

Gonzalez-Zulueta M, Dawson VL, Dawson TM. 1999. Histochemical analysis of nitric oxide synthase by NADPH diaphorase staining. Curr Protocol Toxicol, unit 10.6, DOI: 10.1002/0471140856.tx1006s01.

Halsell CB, Travers SP. 1997. Anterior and posterior oral cavity responsive neurons are differentially distributed among parabrachial subnuclei in rat. J Neurophysiol 78: 920–938.

Halsell CB, Travers SP, Travers JB. 1996. Ascending and descending projections from the rostral nucleus of the solitary tract originate from separate neuronal populations. Neuroscience 72:185–197.

Hamilton RB, Norgren R. 1984. Central projections of gustatory nerves in the rat. J. Comp Neurol 222:560–577.

Harrer MI, Travers SP. 1996. Topographic organization of Fos-like immunoreactivity in the rostral nucleus of the solitary tract evoked by gustatory stimulation with sucrose and quinine. Brain Res 711:125–137.

Hayakawa T, Takanaga A, Tanaka K, Maeda S, Seki M. 2003. Ultrastructure of the central subnucleus of the nucleus tractus solitarii and the esophageal afferent terminals in the rat. Anat Embryol 206:273–281.

Hayato R, Ohtubo Y, Yoshii K. 2007. Functional expression of ionotropic receptors on mouse taste bud cells. J Physiol 584:473–488.

Herbert H, Moga MM, Saper CB. 1990. CB Connections of the parabrachial nucleus with the nucleus of the solitary tract and the medullary reticular formation in the rat. J Comp Neurol 293:540–580.

Hermes SM, Mitchell JL, Aicher SA. 2006. Most neurons in the nucleus tractus solitarii do not send collateral projections to multiple autonomic targets in the rat brain. Exp Neurol 198:539–551.

Higgins GA, Hoffman GE, Wray S, Schwaber JS. 1984. Distribution of neurotensin-immunoreactivity within baroreceptive portions of the nucleus of the tractus solitarius and the dorsal vagal nucleus of the rat. J Comp Neurol 226: 155–164.

Ishida Y, Ugawa S, Ueda T, Yamada T, Shibata Y, Hondoh A, Inoue K, Yu Y, Shimada S. 2009. $P2X_2$- and $P2X_3$-positive fibers in fungiform papillae originate from the chorda tympani but not the trigeminal nerve in rats and mice. J Comp Neurol 514:131–144.

Jones EG. 2005. Allen Online brain atlas: *Mus musculus*. BrainMaps.org.

Kachele DL, Lasiter PS. 1990. Murine strain differences in taste responsivity and organization of the rostral nucleus of the solitary tract. Brain Res Bull 24:239–247.

Kalia M, Sullivan JM. 1982. Brainstem projections of sensory and motor components of the vagus nerve in the rat. J Comp Neurol 211:248–265.

Kanjhan R, Housley GD, Burton LD, Christie DL, Kippenberger A, Thorne PR, Luo L, Ryan AF. 1999. Distribution of the $P2X_2$ receptor subunit of the ATP-gated ion channels in the rat central nervous system. J Comp Neurol 407:11–32.

Karimnamazi H, Travers SP, Travers JB. 2002. Oral and gastric input to the parabrachial nucleus of the rat. Brain Res 957:193–206.

Kestler C, Neuhuber WL, Raab M. 2009. Distribution of $P2X_3$ immunoreactivity in myenteric ganglia of the mouse esophagus. Histochem Cell Biol 131:13–27.

Kim M, Chiego DJ Jr, Bradley RM. 2004. Morphology of parasympathetic neurons innervating rat lingual salivary glands. Auton Neurosci 111:27–36.

King MS and Bradley RM. 1994. Relationship of structure and function of neurons in the rat rostral nucleus tractus solitarii. J Comp Neurol 344:50–64.

Kinzeler NR, Travers SP. 2008. Licking and gaping elicited by microstimlation of the nucleus of the solitary tract. Am J Physiol Regul Integr Comp Physiol 295:R436–R448.

Luppi P-H, Fort P, Jouvet M. 1990. Iontophoretic application of unconjugated cholera toxin B subunit (CTb) combined with immunohistochemistry of neurochemical substances: a method for transmitter identification of retrogradely labeled neurons. Brain Res 534:209–224.

Ma X, Abboud FM, Chapleau MW. 2002. Analysis of afferent, central, and efferent components of the baroreceptor reflex in mice. Am J Physiol Regul Integr Comp Physiol 283:R1033–1040.

May OL, Hill DL. 2006. Gustatory terminal field organization and developmental plasticity in the nucleus of the solitary tract revealed through triple-fluorescence labeling. J Comp Neurol 497:658–669.

McCaughey S. 2007. Taste-evoked responses to sweeteners in the nucleus of the solitary tract differ between C57BL/6ByJ and 129P3/J mice. J Neurosci 27:35–45.

Monroe S, Di Lorenzo PM. 1995. Taste responses in neurons in the nucleus of the solitary tract that do and do not project to the parabrachial pons. J Neurophysiol 74:249–257.

Morest DK. 1960. A study of the structure of the area postrema with Golgi methods. Am J Anat 107:291–303.

Morest DK. 1967. Experimental study of the porjections of the nucleus of the tractus solitaries and the area postrema in the cat. J Comp Neurol 130:277–300.

Nasse J, Terman D, Venugopal S, Hermann G, Rogers R, Travers JB. 2008. Local circuit input to the medullary reticular formation from the rostral nucleus of the solitary tract. Am J Physiol Regul Integr Comp Physiol 295:R1391–R1408.

Nelson G, Hoon MA, Chandrashekar J, Zhanf Y, Ryba NJP, Zuker CS. 2001. Mammalian sweet taste receptoprs. Cell 106:381–390.

Nomura S, Mizuno N. 1981. Central distribution of afferent and efferent components of the chorda tympani in the cat as revealed by the horseradish peroxidase method. Brain Res 214:229–237.

Nomura S, Mizuno N. 1983. Central distribution of afferent fibers in the intermediate nerve: a transganglionic HRP study in the cat. Neurosci Lett 41:227–231.

Norgren R. 1978. Projections from the nucleus of the solitary tract in the rat. Neuroscience 3:207–218.

Norgren R, Leonard CM. 1973. Ascending central gustatory pathways. J Comp Neurol 150:217–238.

Ohmoto M, Matsumoto I, Yasuoka A, Yoshihara Y, Abe K. 2008. Genetic tracing of the gustatory and trigeminal neural pathways originating from T1R3-expressing taste receptor cells and solitary chemoreceptor cells. Mol Cell Neurosci 38:505–517.

Okada T, Tashiro Y, Kato F, Yanagawa Y, Obata K, Kawai Y. 2008. Quantitative and immunohistochemical analysis of neuronal types in the mouse caudal nucleus tractus solitarius. Chem Neuroanat 35:275–284.

Paton JF. 1998a. Pattern of cardiorespiratory afferent convergence to solitary tract neurons driven by pulmonary vagal C-fiber stimulation in the mouse. J Neurophysiol 79:2365–2373.

Paton JF. 1998b. Convergence properties of solitary tract neurons driven synaptically by cardiac vagal afferents in the mouse J Physiol 508:237–252.

Paxinos G, Franklin KBJ. 2001. The mouse brain in stereotaxic coordinates, 2nd ed. New York: Academic Press.

Paxinos G, Watson C. 2007. The rat brain in stereotaxic coordinates, 6th ed. New York: Academic Press.

Ramón y Cajal S. 1972. Histologie du système nerveux de l'homme et des vértebrés, vol 1. Azoulay L, translator. Madrid: Insituto Ramón y Cajal.

Ross CA, Ruggiero DA, Reis DJ. 1985. Projections from the nucleus tractus solitarii to the rostral ventrolateral medulla. J Comp Neurol 242:511–534.

Sang Q, Goyal RK. 2001. Swallowing reflex and brain stem neurons activated by superior laryngeal nerve stimulation in the mouse. Am J Physiol Gastrointest Liver Physiol 280:G191–G200.

Scherer-Singler U, Vincent SR, Kimura H, McGeer EG. 1983. Demonstration of a unique population of neurons with NADPH-diaphorase histochemistry. J Neurosci Methods 9:229–234.

Siegel S, Castellan NJ Jr. 1988. Nonparametric statistics for the behavioral sciences, 2nd ed. New York: McGraw-Hill, p 213–215.

Sugita M, Shiba Y. 2005. Genetic tracing shows segregation of taste neuronal circuitries for bitter and sweet. Science 309:781–785.

Suwabe T, Bradley RM. 2009. Characteristics of convergent synaptic activity between the caudal brainstem gustatory nucleus and neurons in the chorda tympani terminal field projecting to the parabrachial nucleus. AChemS 31st Annual Meeting, Sarasota, FL, abstract P47, p 41.

Terai K, Tooyama I, Kimura H. 1997. Immunohistochemical localization of $GABA_A$ receptors in comparison with GABA-immunoreactive structures in the nucleus tractus solitarii of the rat. Neuroscience 82:843–852.

Tokita K, Inoue T, Boughter JD Jr. 2009. Afferent connections of the parabrachial nucleus in C57BL/6J mice. Neuroscience 161:475–488.

Tokita K, Yamamoto T, Boughter JD. 2012. Gustatory neural responses to umami stimuli in the parabrachial nucleus of C57BL/6J mice. J Neurophysiol 107:1545–1555.

Travers JB. 1988. Efferent projections from the anterior nucleus of the solitary tract of the hamster. Brain Res 457:1–11.

Travers SP, Hu H. 2000. Extranuclear projections of rNST neurons expressing gustatory-elicited Fos. J Comp Neurol 427:124–138.

Travers SP, Norgren R. 1995. Organization of orosensory responses in the nucleus of the solitary tract in the rat. J Neurophysiol 73:2144–2162.

Travers SP, Travers JB. 2007. Taste-evoked Fos expression in nitrergic neurons in the nucleus of the solitary tract and reticular formation of the rat J Comp Neurol 500:746–760.

Travers JB, Herman K, Yoo J, Travers SP. 2007. Taste reactivity and Fos expression in GAD1-EGFP transgenic mice. Chem Senses 32:129–137.

Vercelli A, Repici M, Garbossa D, Grimaldi A. 2000. Recent techniques for tracing pathways in the central nervous system of developing andf adult animals. Brain Res Bull 51:11–28.

Wang M, Bradley RM. 2010. Properties of GABAergic neurons in the rostral solitary tract nucleus in mice. J Neurophysiol 103:3205–3218.

Wang Z-J, Neuhuber WL. 2003. Intraganglionic laminar endings in the rat esophagus contain $P2X_2$ and $P2X_3$ receptor immunoreactivity. Anat Embryol 207:363–371.

Whitehead MC. 1988. Neuronal architecture of the nucleus of the solitary tract in the hamster. J Comp Neurol 276: 547–572.

Whitehead MC. 1990. Subdivisions and neuron types of the nucleus of the solitary tract that project to the parabrachial nucleus in the hamster. J Comp Neurol 301:554–574.

Whitehead MC, Finger TE. 2008. Gustatory pathways in fish and mammals. In Firestein S, Beauchamp G, editor. The senses: a comprehensive reference, vol. 4, olfaction and taste. Oxford: Elsevier. p 237–259.

Whitehead MC, Frank ME. 1983. Anatomy of the gustatory system in the hamster: central projections of the chorda tympani and the lingual nerve. J Comp Neurol 220:378–395.

Whitehead MC, Bergula A, Holliday K. 2000. Forebrain projections to the rostral nucleus of the solitary tract in the hamster. J Comp Neurol 422:429–447.

Williams JB, Murphy DM, Reynolds KE, Welch SJ, King MS. 1996. Demonstration of a bilateral projection from the rostral nucleus of the solitary tract to the medial parabrachial nucleus in rat. Brain Res 737:231–237.

Yamamoto K, Ishimaru Y, Ohmoto M, Matsumoto I, Asakura T, Abe K. 2011. Genetic tracing of the gustatory neural pathway originating from Pkd1l3-expressing type III taste cells in circumvallate and foliate papillae. J Neurochem 119:497–506.

Yao ST, Barden JA, Lawrence AJ. 2001. On the immunohistochemical distribution of ionotropic P2X receptors in the nucleus tractus solitarius of the rat. Neuroscience 108: 673–685.

Zaidi FN, Todd K, Enquist L, Whitehead MC. 2008. Types of taste circuits synaptically linked to a few geniculate ganglion neurons. J Comp Neurol 511:753–772.

Zhang L-L, Ashwell KW. 2001. Development of the cyto- and chemoarchitectural organization of the rat nucleus of the solitary tract. Anat Embryol 203:265–282.

Zhang J, Walker JF, Gurardiola J, Yu J. 2006. Pulmonary sensory and reflex responses in the mouse. J Appl Physiol 101:986–992.